NTIA Report 83-128

A Diagnostic Probe to Investigate Propagation at Millimeter Wavelengths

E.J. Violette
R.H. Espeland
K.C. Allen

U.S. DEPARTMENT OF COMMERCE
Malcolm Baldrige, Secretary
David J. Markey, Assistant Secretary
for Communications and Information

August 1983

TABLE OF CONTENTS

LIST OF FIGURES

A DIAGNOSTIC PROBE TO INVESTIGATE PROPAGATION AT MILLIMETER WAVELENGTHS

E. J. Violette, R. H. Espeland, and K. C. Allen*

A diagnostic probe used to fully describe the propagation characteristics of a millimeter wave channel by nearly simultaneous recording of an impulse response, frequency spectra, amplitude response, and bit error rate is discussed. A 30.3 GHz carrier accommodates the subcarriers and baseband modulation modes in a fully coherent network. Signal-to-noise determining components will permit BER performance of better than 10^{-8} at a 500 Mb/s rate with a 25 dB fade margin through a clear air 50 km distortion free path. Back to back operation of the terminals and a short atmospheric path is used to establish the reference performance level of the hardware. Controlled multipath tests are reported to demonstrate probe capabilities and to obtain reference data to better classify the fades and resulting distortion which occur on terrestrial links at millimeter wavelengths. With dual reflectors, multipath data sets were compiled to aid in predicting bit error rate performance resulting from a combination of signal-to-noise ratio change and intersymbol interference. Included with the above data are corresponding measurements of the impulse response and amplitude distortion on the channel. Two additional coherent cw channels, 11.4, 28.8, and a soon to be added 96.1 GHz channel, are included with the 30.3 GHz probe to aid in analyzing selective fades which fall outside the bandpass and to evaluate frequency dependent properties of a link.

Key words: diagnostic; digital; millimeter waves; propagation; probe; wide-band

1. INTRODUCTION

The diagnostic probe has been instrumented to obtain a better understanding of the millimeter wave (mm-wave) channel through the atmospheric medium, especially for wide band applications. Nearly all applications with the mm-wave terminals separated by at least a far field distance can be analyzed by the probe. Propagation characteristics of a path, which are of concern to a user, include those properties that change the received signal amplitude or transit time for any frequency within the bandpass of the system. The basic parameter in predicting link performance is the achievable signal-to-noise ratio (S/N) and its time variability caused by propagation factors acting on the transmitted signal. Also of particular interest, especially as system bandwidths increase, are factors that contribute to signal distortion. For a terrestrial line-of-sight link, path geometry and climate are important factors in predicting channel distortion. Objects mutually illuminated

---

*The authors are with the U.S. Department of Commerce, National Telecommunications and Information Administration, Institute for Telecommunication Sciences, Boulder, CO 80303.

by the antenna of each terminal produce delayed signals or multipath signals by means of reflection, refraction, or diffraction that combine at the receiving antenna to modify both the amplitude and phase of the direct signal.

The atmosphere is a nonhomogeneous medium, constantly in some degree of motion, which bends the transmitted rays to create signal scintillation, atmospheric multipath, ray focusing (or defocusing), and/or angle of arrival fluctuations. These effects are most pronounced in wide-band millimeter wave propagation and their severity depends on meteorological parameters. The amount of ray bending by an atmospheric refractive gradient is not a function of frequency, but at higher frequencies, these path changes become a larger fraction of the rf wavelength producing phase interference and dispersion across the channel bandwidth.

One of the features of the diagnostic probe is the ability to measure the impulse response of the channel. This is accomplished by the phase modulation of a 30.3 GHz carrier with a pseudorandom binary sequence at a rate of 500 Mb/s. The 30.3 GHz signal is transmitted through the channel to a receiver where the signal is demodulated to reproduce the 500 Mb/s pseudorandom sequence degraded by any distortion that may have occurred in the propagation between transmitter and receiver. At the receiver terminal, a replica of the transmitted pseudorandom binary sequence is generated. A cross-correlation is performed between the received demodulated bit stream and the replica of the transmitted bit stream by allowing one bit stream to slide by the other in time as a result of a slight offset in the bit-clock frequencies. At the point in time when the bit sequences are identically aligned, an impulse is generated with a base duration equal to two bit times. The impulse response measurement repeats at a rate corresponding to the number of bits in the sequence or word divided by the clock offset rate. Channel amplitude and phase dispersion during propagation of the signal appear as amplitude and time changes in the impulse shape. A channel is completely described by the channel impulse response or its Fourier transform, the transfer function of the channel. Thus, the diagnostic probe is a means of acquiring data to determine parameters in modeling channel characteristics and predicting performance for specific applications.

In near real time, the received bit stream can be routed for processing by matched filters and decision making circuitry to estimate the binary states of the received data stream. With knowledge of the transmitted word, a count of the occurrence of errors can be recorded. This permits a performance measure of a channel in terms of bit error rate (BER) which can be compared to channel characteristics as seen by the impulse probe.

To provide a complete diagnosis of a channel and improve measurement accuracy, amplitude response information across the channel bandwidth is desirable. The high data rate of 500 Mb/s and the relatively long pseudorandom word lengths (2^7 or 2^{15} bits) provide a wide bandwidth (1 GHz) with closely spaced spectrum lines (4 MHz or 15 kHz correspondingly), so that amplitude distortion of a channel can be viewed with high resolution. This is particularly useful for channels containing multipath signals that produce selective fades. An amplitude response display across the bandwidth shows the relative location of fade nulls which are not as easily obtained from the impulse probe and is important in analyzing short-term (millisecond to seconds) link performances.

2. DESCRIPTION OF PROBE

2.1 Transmitter Terminal

Figure 2.1 shows a block diagram of the transmitter terminal of the probe which is contained in two enclosures. One houses the hardware that generates the rf signals fed to the antennas and the other houses the baseband data generators and modulators to provide the 1.5 GHz modulated subcarrier. To avoid problems with beat frequency components and relative phase shifts, all signals are derived from a single temperature compensated crystal oscillator (TCXO). All active multipliers are phase-locked and those with outputs at microwave frequencies are cavity tuned to reduce the noise bandwidth. The blocks shown in Figure 2.1 with the heavy line at the base indicate those units with active components.

The Gunn effect source is injection locked through a circulator and supplies an output of 150 mW at 28.8 GHz for the upconverter local oscillator and the cw probe output. With 10 mW of subcarrier at 1.5 GHz, the upconverter generates a 30.3 GHz carrier with modulation at 1 mW of upper sideband (USB) power after the low-pass reject filter. A flat ($\pm$ 2 dB) bandwidth of 2 GHz has been achieved with the balanced mixer and computer-designed etched filter, which is a key element in generating a sum of the input signals with the low distortion necessary to maintain a high resolution probe. Another critical element is in the design of a Ka band power amplifier. The 1 mW is increased to 100 mW with a high degree of amplitude flatness and phase linearity across the 29 to 31 GHz portion of the 26 to 38 GHz response range of the power amplifier. The power rating of this amplifier increased the useful range of the wideband probe to at least 50 km. The antennas typically used on the 30.3 GHz link are 3-foot parabolic reflectors (0.75° beamwidth) with feeds that provide dual linear polarization. Isolation between orthogonal linear modes is better than 38 dB allowing depolarization measurements for many path conditions.

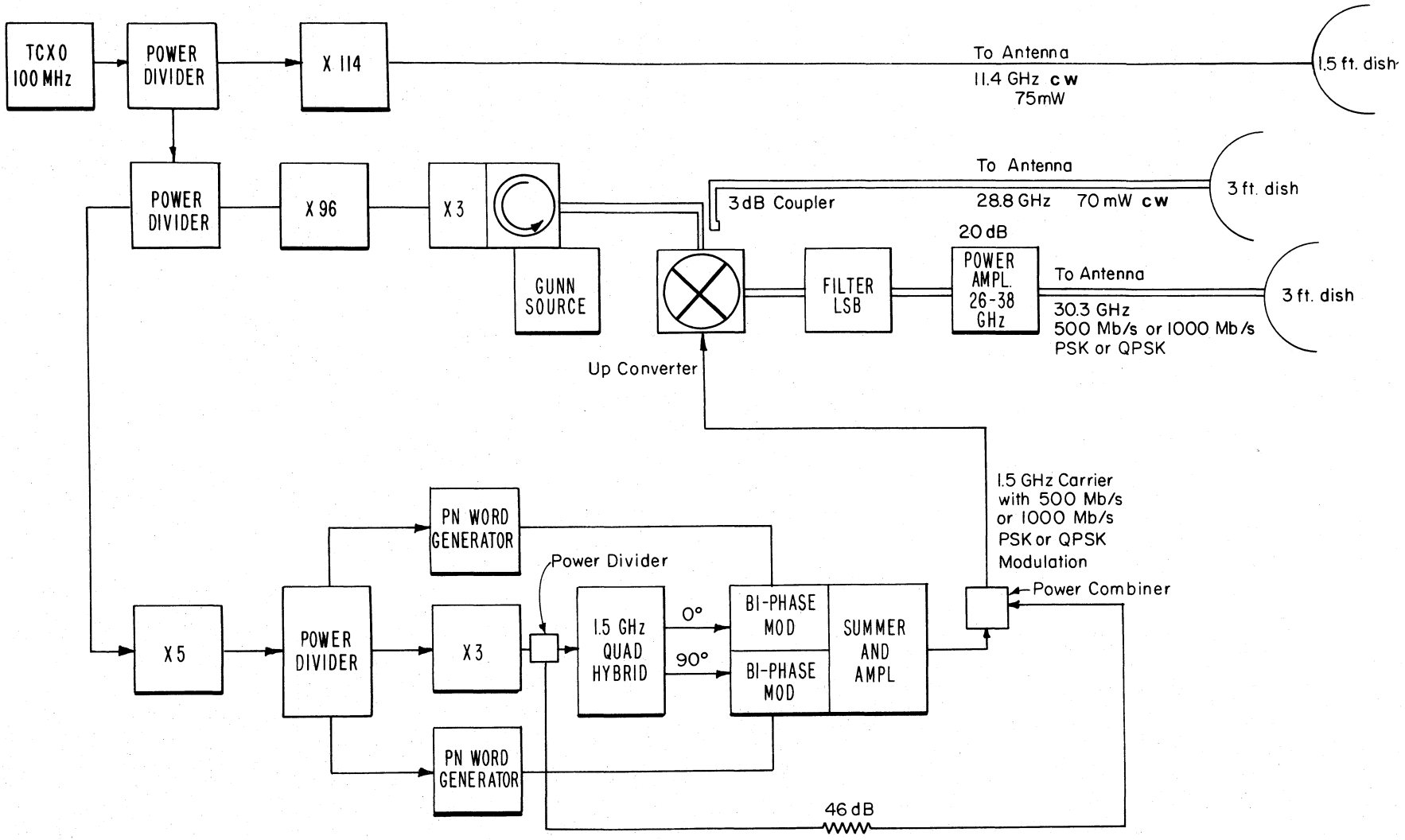

Figure 2.1 Block diagram of the transmitter terminal.

The baseband digital generators are capable of producing a pseudorandom data stream at rates from 200 to 1000 Mb/s. Because of matched filters and decision circuitry at the demodulator, a fixed data rate is required. For all bit error rate (BER) diagnostic applications a rate of 500 Mb/s is used. Pseudorandom code lengths or word lengths of either 2^7-1 (127 bits) or 2^{15}-1 (32,767 bits) can be selected. One or both data streams from the word generator can be applied to quadrature components of a 1.5 GHz subcarrier, summed, and amplified to provide a 10 mW drive to the upconverter. Thus, in the fixed rate case, the carrier is modulated in either a 1000 Mb/s quadraphase shift key (QPSK) mode or a 500 Mb/s biphase shift key (BPSK) mode depending on the probe applications.

2.2 Receiver Radio Frequency Portion

A block diagram of the rf portion of the receiver is shown in Figure 2.2. The first-stage downconverter and integrated preamplifier is a balanced mixer, using Strip-Guide design, direct coupled to a low-noise linear amplifier with a 3 dB noise figure. This combination has a single sideband effective noise figure of less than 8 dB with 24 dB ($\pm$ 1 dB) gain and $\pm$ 7 degrees phase linearity over a 1.5 GHz bandwidth. Generation of the local oscillator signal is from a 100 MHz voltage controlled crystal oscillator (VCXO), a X96 phased-locked cavity-tuned multiplier, and a passive harmonic tripler all selected for their low phase noise. All received IF signals are phased-locked to the transmitted signal by controlling a 100 MHz VCXO which is used to generate the local oscillator (L.O.) reference for each rf down-converter. The purpose of the cw probes is to isolate frequency dependent parameters of a transmission channel. As indicated in Figure 2.2, dual antennas are employed with the cw probes (a wide beamwidth and a narrow beamwidth) in order to isolate angle of arrival or beam decoupling fades from other sources of fades. Also, the two-beam link enables some determination to be made on direction and type of multi-path present, especially those associated with paths generated by refractive bending of rays. When the narrow beam antenna is pointed for ground clearance and no fading is seen, but the widebeam channel shows fading, then multipath signals are assumed. If both beams show fading, then atmospheric multipath is assumed.

2.3 Demodulator S/N Performance Tester

Figure 2.3 presents a block diagram of the demodulator portion of the wide-band probe. It consists of a S/N performance tester which primarily allows white noise to be mixed with the modulated 1.5 GHz input signal or at baseband frequencies to calibrate the BER in terms of the ratio of bit energy to noise energy (E_b/N_o) for either of the bands in question.

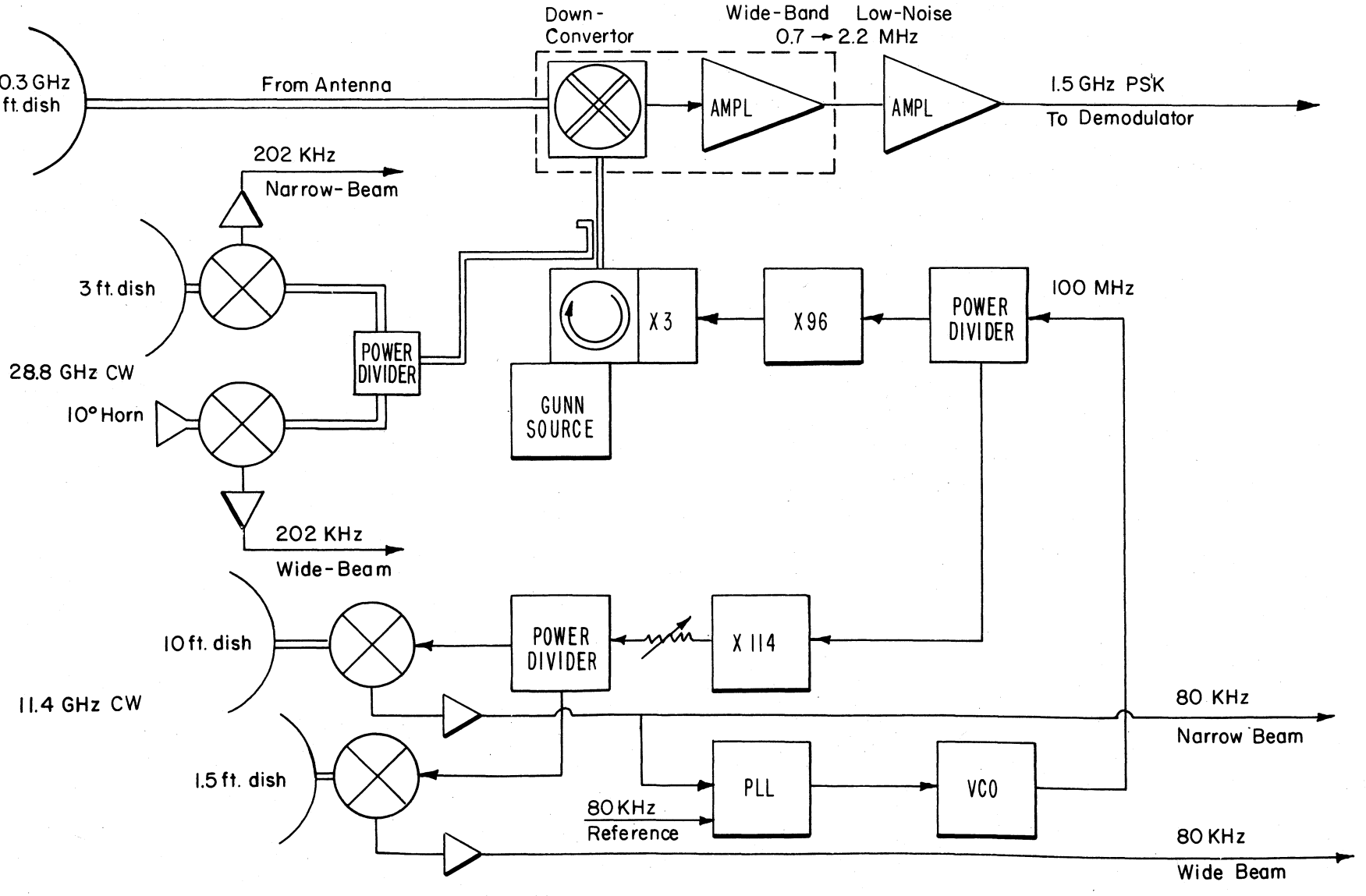

Figure 2.2 Block diagram of the rf section of the receiver terminal.

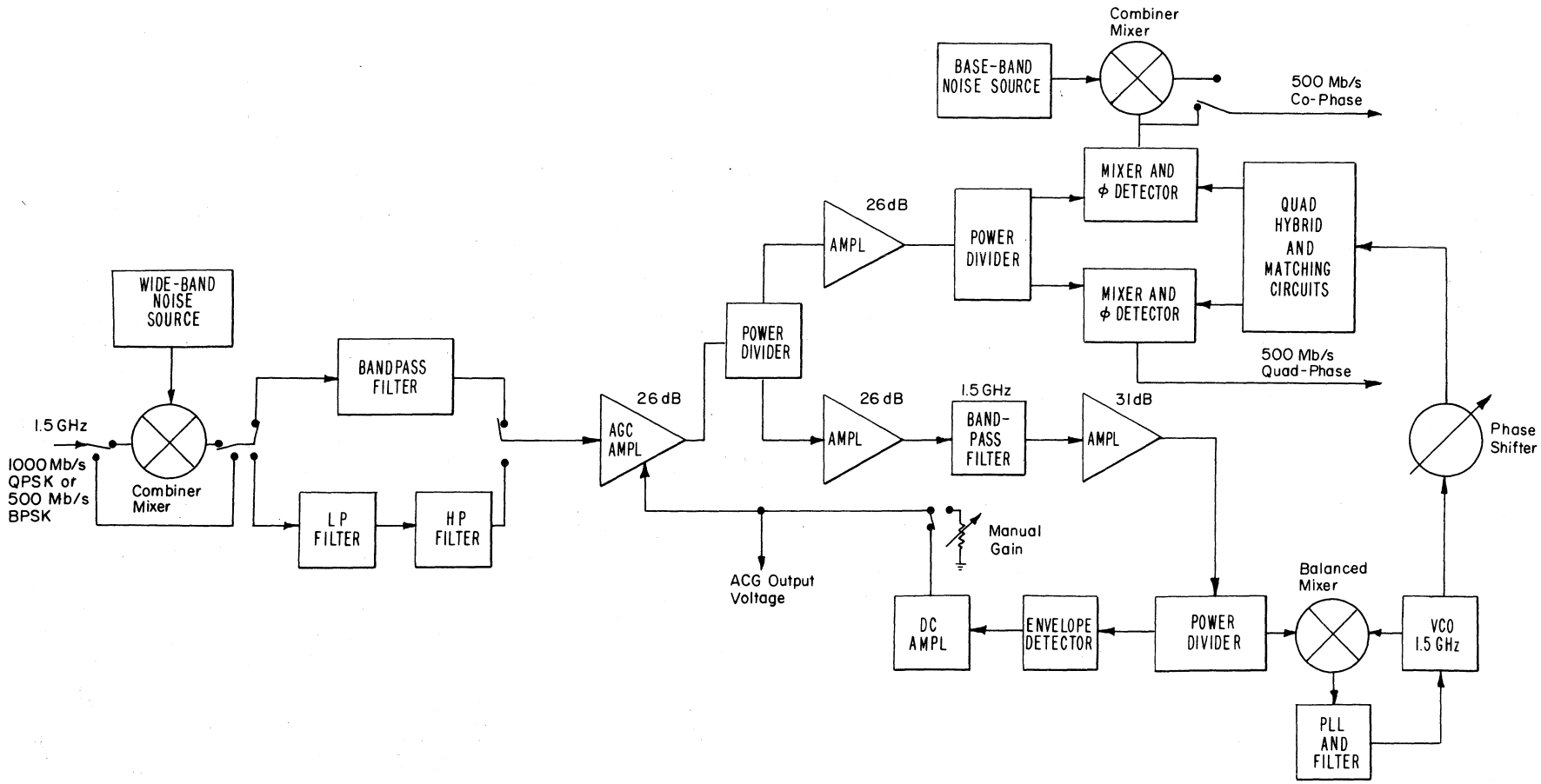

Figure 2.3 Block diagram of the receiver demodulator.

The 1.5 GHz modulated carrier is filtered, amplified by the 24 dB gain controlled circuit and then divided. The upper branch is again amplified, divided and fed into the baseband mixer-detectors to provide a co-phase and a quad-phase channel. When measuring the channel impulse response, a BPSK transmission is used to permit a sum of the squares operation at the co- and quad-phase channels to accurately measure the amplitude for all phase combinations of the incoming signals.

The lower branch of the modulated 1.5 GHz signal is likewise amplified and divided for use in the carrier reconstruction and automatic gain control (AGC) circuitry. Carrier reconstruction is accomplished by inserting a small subcarrier signal (30 dB below the total power in band) at the modulator to serve as a source to phase-lock a voltage controlled oscillator (VCO). A narrowband phase-tracking loop greatly improves the signal-to-noise ratio (S/N) which reflects in a lower BER. The output of the VCO is passed through a phase shifter then split into quadrature phase components to properly regenerate the baseband data stream at the mixer phase-detector. To insure a proper in-phase and quad-phase relationship of the 1.5 GHz VCO reference, relative to the modulated signal phase at the detector, the AGC circuit adjusts the amplifier gain for a constant output from the first demodulator amplifier. A constant phase is held by this AGC action over a 20 dB range of received signal level. Programmable attenuators (Figure 2.6) are used at the demodulator input to extend the range of the input signal level (with constant phase to the detector) beyond the 20 dB range of the AGC amplifier. One of the diagnostic parameters is the AGC voltage, calibrated to give a dBm level for the received signal. The AGC voltage indicates signal plus noise power over a $\pm$ 350 MHz bandwidth centered at 1.5 GHz.

2.4 Bit Synchronizer and Signal Conditioner

Functional diagrams of the bit synchronizer-signal conditioner (BSSC) and bit error detector circuitry are shown in Figure 2.4. The design of the BSSC is the result of an engineering development done for Air Force Avionics Laboratory Wright-Patterson AFB on Contract Number F33615-73-C-1026. A discussion of the techniques used are contained in Gray (1969) and Gray (1972).

2.5 Bit Error Detector

A functional diagram of the bit error detector is included in Figure 2.4. The unit used for this purpose is a wide-band digital receiver with an input range of from 200 to 1000 Mb/s. Internally the data estimate is shaped and demultiplexed to 1/4 rate to allow compatibility with commerically available high speed emitter-coupled-logic integrated circuits. An error detector module processes the

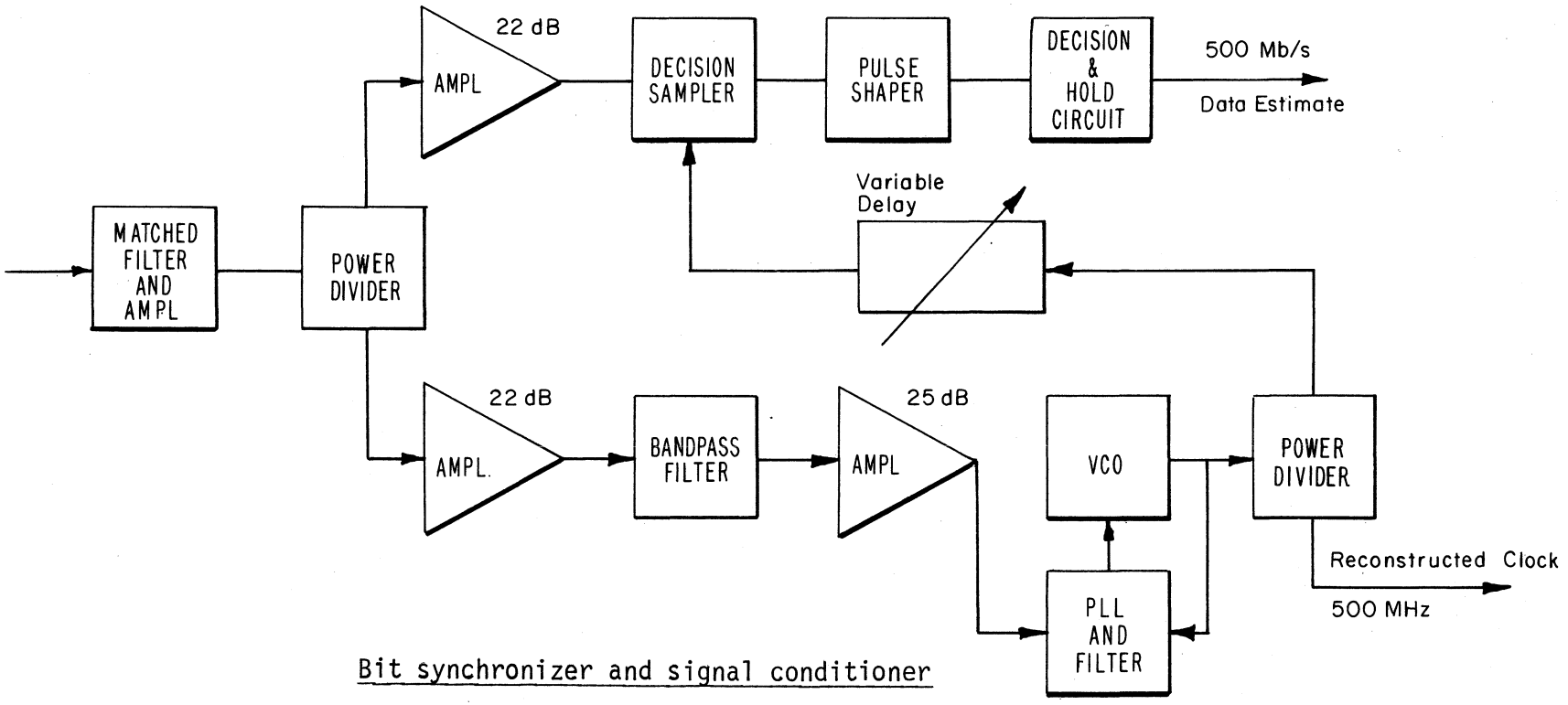

Bit synchronizer and signal conditioner

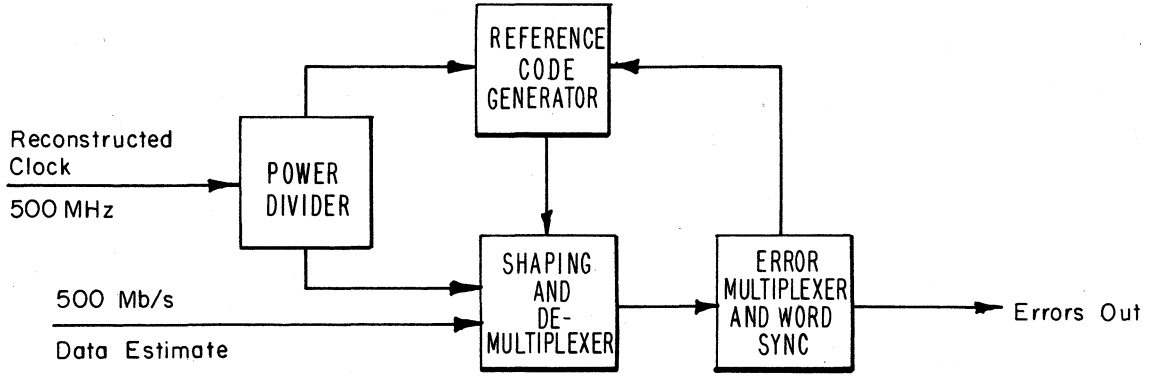

Bit error receiver

Figure 2.4 Block diagram of the bit synchronizer, signal conditioner, and bit error receiver.

demultiplexed signals and does a parallel bit-by-bit comparison between the locally generated 4-phase signal and the 4-phase signal derived from the input signal. Automatic synchronization occurs by counting successive zeros in the data stream and latches the internal bit clock when this number reaches n-1, where n is the number of stages in the data generator shift register. Synchronization acquisition is based on the definition of fewer than 30,000 errors in an 80,000 bit frame of received data. This also defines an out of sync condition and describes the maximum error burst detectable. The error output is fed to a gated counter which is sampled by the data logging computer at a 1-second interval establishing the minimum detectable error rate at 2×10^{-8}. An ungated counter is used as a totalizer to obtain values for lower error rates.

2.6 Theory of Cross-Correlator Impulse Response Probe

A short explanation of how the cross-correlation of the transmitted and received pseudo-random bit streams is a measure of the channel impulse response is given below. For a rigorous analysis and background theory of pseudo-random channel probe measurements, Linfield et al., (1976) and Hufford et al., (1982) are recommended.

That the cross-correlation is a measure of the impulse response can be seen as follows. Note first that the received baseband bit sequence, $y(t)$, is just the transmitted baseband sequence, $x(t)$, convolved with the channel impulse response, $h(t)$

$$y(t) = x(t) * h(t) \ .$$

Here $h(t)$ is complex because $y(t)$ and $x(t)$ are baseband signals. At the receiver the cross-correlation, $R_{xy}(\tau)$, of the received bit sequence with the replica of the transmitted sequence is found. Since the correlation operation is equivalent to a convolution, with one of the functions time inverted, the measured cross-correlation is a triple convolution; i.e.,

$$R_{xy}(\tau) = x(t) * y(t) = x(-t) * x(t) * h(t) \ .$$

The order of the convolutions does not change the result. Thus, the cross-correlation is equivalent to the correlation of the psuedo-random bit sequence with itself, convolved with the channel impulse response. But the auto-correlation of the transmitted bit sequence is a triangular shaped pulse $P(t)$,

$$P(t) = x(-t) * x(t),$$

with rounded corners because of the bandwidth limitations of the system. The base of the triangle is equivalent to two bit durations. Thus, the cross-correlation is

the impulse response of the channel convolved with or smoothed by this triangular shaped pulse,

$$R_{xy}(\tau) = P(t) * h(t)$$

It can be seen that a higher data rate or greater bandwidth system allows higher resolution measurements of the impulse response because the auto-correlation of the transmitted signal is narrower in time.

It should be noted that $R_{xy}(\tau)$ is complex valued due to the rotation of the impulse response into the complex plane when the transition to the baseband is made. Since the true impulse response of the channel is real valued, it is the magnitude of h(t) which is of interest. Thus, the sum of the squares operation is performed on the cross-correlation.

2.7 Impulse Response Cross-Correlator

The impulse response mode can be requested by the computer or by manual command. A function diagram of the cross-correlator for the impulse mode is shown in Figure 2.5. The correlator best suited to the purpose is an extended frequency range (1 to 1000 MHz) double-balanced mixer. Since a positive or negative level occurs at the mixer output depending on the phase of the received signal, a co- and quadrature-phase data stream is generated in the demodulator so that the sum of the squares operation can be performed to obtain the proper magnitude of the impulse response curve (the power impulse function). Each correlator is driven as a local oscillator by a 2^n bit word generator which creates a replica of the signal transmitted. An offset frequency clocks the replica generator with a rate of a few hertz (rate depends on word length 2^7-1 or 2^{15}-1) slower than the transmitted bit clock so that in roughly a 1-second period, all bits in the replica word slide by the received word. When all the ones and zeros within the two words coincide, a triangular impulse voltage waveform occurs with a normalized peak to base amplitude equal to $1/2^n$-1 providing a maximum dynamic range of about 42 dB for the 2^7-1 word length and and 90 dB for the 2^{15}-1 word length. Because a 3-1/2 digit voltmeter was the best available for the high sampling rate required, the dynamic range of the measurement is restricted to 30 dB. This minimum recordable voltage level falls above the noise threshold of the 30.3 GHz, 500 Mb/s probe until the receiver input level is less than about -76 dBm. As shown later in this report, a multipath signal 30 dB below the direct signal level produces very little degradation of the channel. In fact, voltage standing waves at waveguide or coax connections are visible in the impulse response curves.

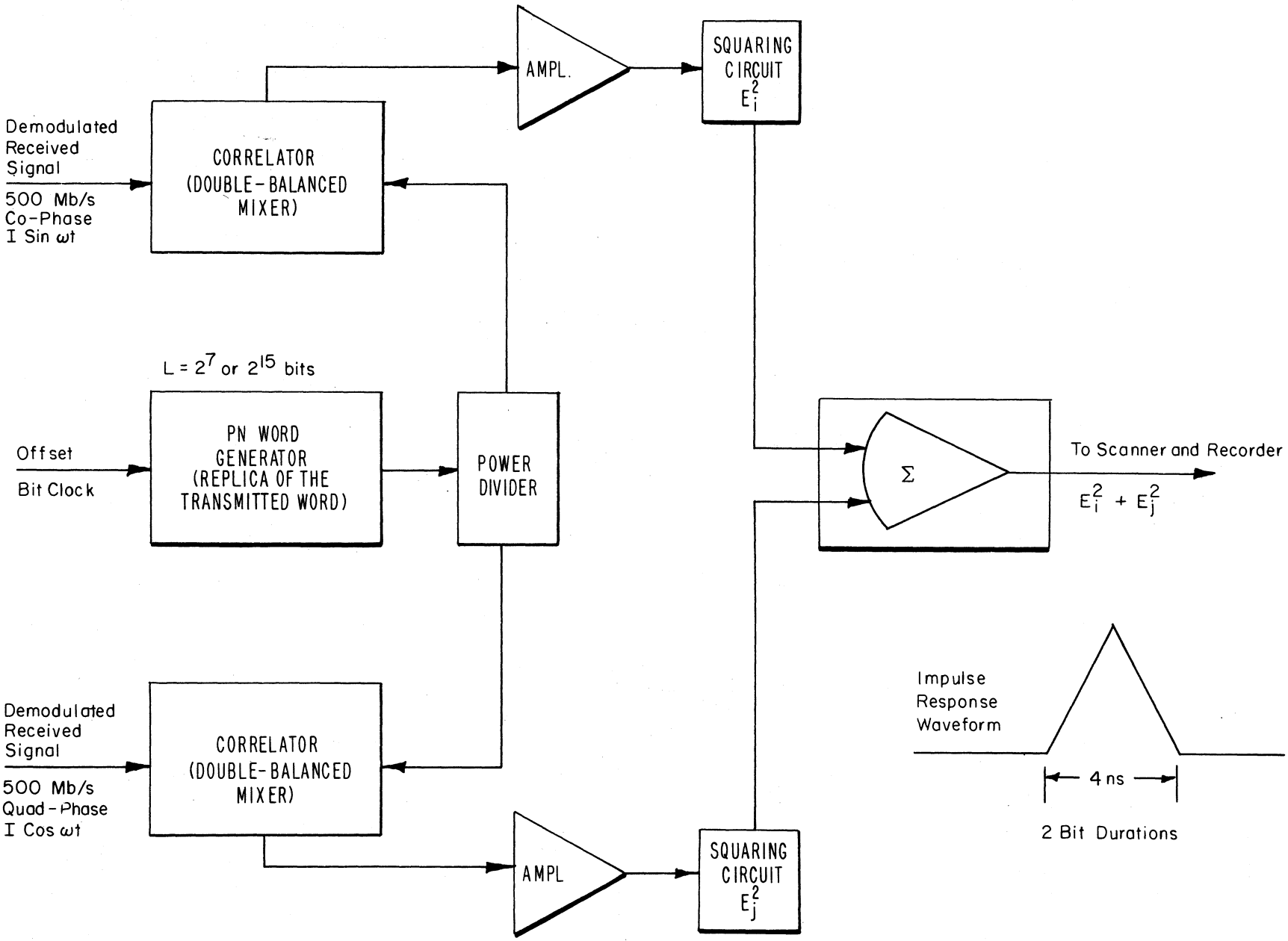

Figure 2.5 Block diagram of the impulse response cross-correlator.

In the ideal case, the base width of the impulse response curve is 2 bit-time durations (4 ns) but the actual record time for this base width is approximately 15.75 ms ($\frac{2 \text{ bits}}{127 \text{ bits}}$ x 1 second) at a clock offset rate providing an impulse repetition period of 1 per second for the 127 bit word length. This 15.75 ms interval is small compared to atmospherically induced changes which have minimum periods in the order of 0.1 second. Since all circuits used in the correlation process are not perfectly linear, the hardware produces some distortion in the impulse measurements and for this probe an increase in the base width to about 5 ns occurred. The impulse curve generated by the hardware only, becomes the reference to compare channel distortion resulting from an atmospheric path. Any circuit or channel distortion occurring within the impulse time period affects the shape of the impulse. However, any time delayed signal (multipath signal) greater than the one bit clock period shows as a separate delayed impulse with an amplitude that is a function of its contribution to the total received rf power. Examples of these impulse waveforms are shown in Section 5 of this report.

2.8 Computer Controlled Data Acquisition and Recording Equipment

All data logging and recording operations are controlled by a 9845 desk-top computer. Functions controlled by the computer are shown in Figure 2.6. Input signals are sampled by a scanner and read by a high speed 3-1/2 digit voltmeter (4000 readings per second) for processing in the computer. Parameters of the rf channels such as amplitude of the 11.4, 28.8, and 30.3 GHz carriers (a 96.1 GHz carrier is to be added in the near future) can be sampled at up to a 0.1 second rate. Also, channel impulse response measurements can be completed and recorded at 2-second intervals. Meteorological data, which includes air temperature, pressure, and rain rate are generally sampled with the rf amplitude readings. A cavity-type microwave refractometer feeds the computer with N values of $\pm$ 0.1 N resolution each second or $\pm$ 1.0 N resolution in a 0.1 second sampling period. Up to four cavities can be positioned to obtain spatial variations of N. At a 1-second gate-time, a period counter reads BER down to a 2×10^{-8} rate and a 1 MHz to 2 GHz spectrum analyzer with digital memory scans the wide-band probe amplitude response through a yet to be completed interface unit.

Computer programs are fed from either the magnetic tape or floppy disk and each also serves to store the recorded data. Data can be retrieved, processed, and displayed on the plotter connected to the system. Several kinds of software are available for the computer including ray tracing from refractive index profiles to predict channel performance. The basic logging programs monitor the channel signal amplitudes, BER, and meteorological data until the BER exceeds a pre-set threshold

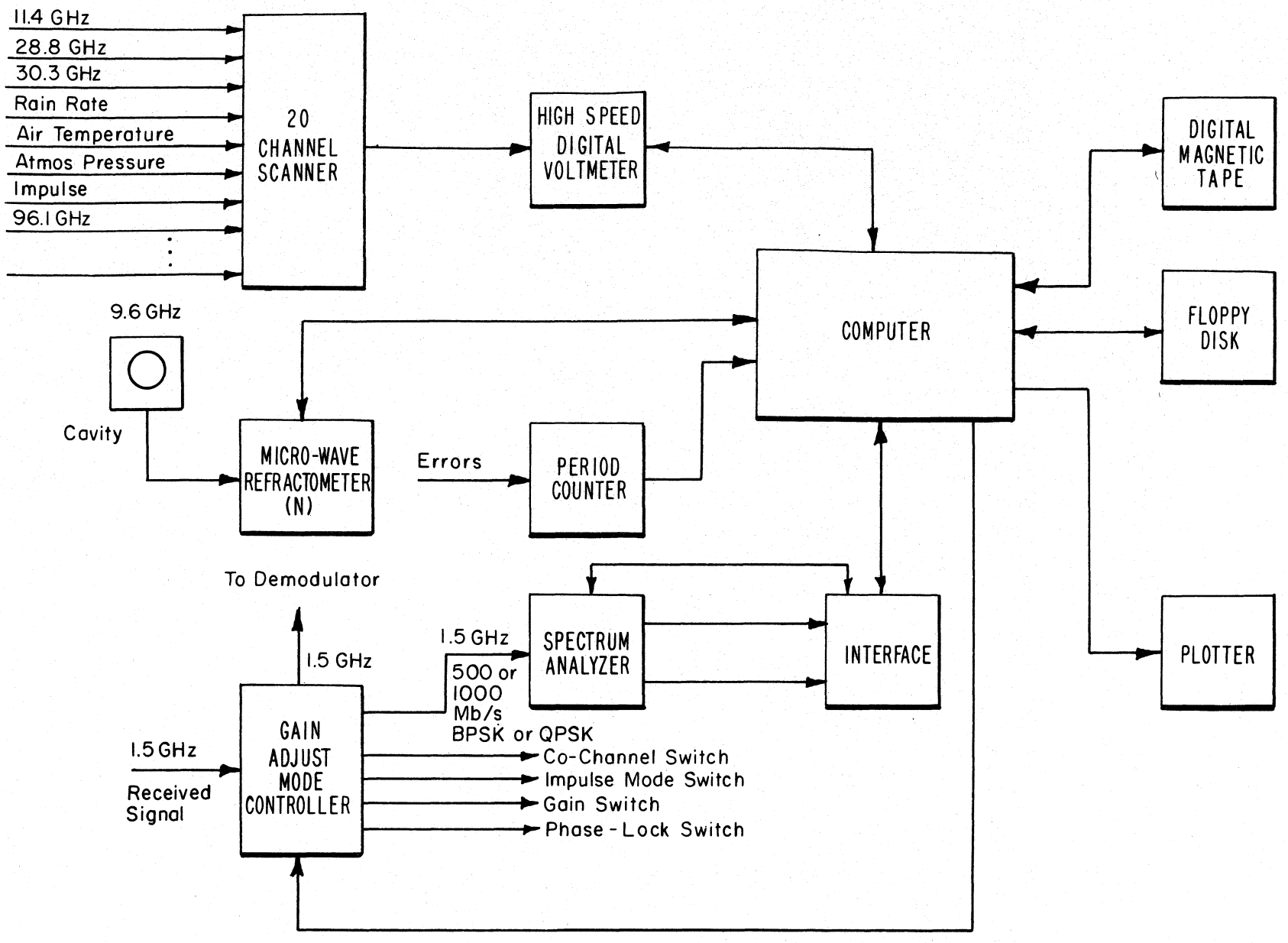

Figure 2.6 Diagram of the data acquisition and recording equipment.

(perhaps 10^{-6}). When it is not raining at the receiving terminal and this threshold is exceeded, it is assumed channel distortion is present and the impulse response and amplitude scans are programmed. A refinement which may be included is the onset timing and the ratio of change of channel attenuation with frequency in real time processing to permit a determination if rain is present on any part of a path. Also, the frequency dependence of rain attenuation permits calculation of rain drop size distribution (Furuhama and Ihara; 1981) which can be compared with season of year, type of storm, rain rate, etc.

3. DIAGNOSTIC PROBE CALIBRATION AND BER PERFORMANCE

A common measure of the performance of a digital modem is in terms of bit error rate (BER) for a given signal-to-noise ratio at the demodulator. By mixing very wide-band noise with the signal at the demodulator input, as accomplished by the link tester, a curve of BER versus S/N can be drawn. This curve is typically compared to the theoretical or ideal performance curve, for coherent BPSK modulation in this case. The theoretical performance curve for a coherent BPSK with additive Gaussian noise is calculated from

$$BER = e^{-E_b/N_o} \; / \; 2\sqrt{\pi \; E_b/N_o}$$

where E_b/N_o is defined as bit signal energy to one-sided noise spectral power density (Wozencraft and Jacobs, 1965). In terms of S/N, the ratio of signal power to noise power in the signal bandwidth is

$$E_b/N_o = S/N + 10 \log \frac{\text{Signal bandwidth (w)}}{\text{bit rate } (R_b)} \quad .$$

For the 500 Mb/s, BPSK, BER measurements, the signal bandwidth is determined by a 1 GHz filter at the demodulator input. Figure 3.1 contains plots of the theoretical curve and measured values of some of the important stages within the system as well as through two rf links. The theoretical curve (#1) represents a distortion free system. With the baseband generator and bit error receiver connected back to back, the E_b/N_o is within 1 dB of theoretical (curve not shown). With the 1.5 GHz PSK subcarrier modulator-demodulator connected back to back (curve #2 of Figure 3.1), the E_b/N_o departs by about 2 dB from theoretical at a BER of 10^{-8}. Considering that 500 MHz logic and switching circuits are near state of the art, this represents an excellent performance level. Utilization of matched filters and decision circuitry developed under sponsorship of the U.S. Air Force (Gray, 1973), contributes

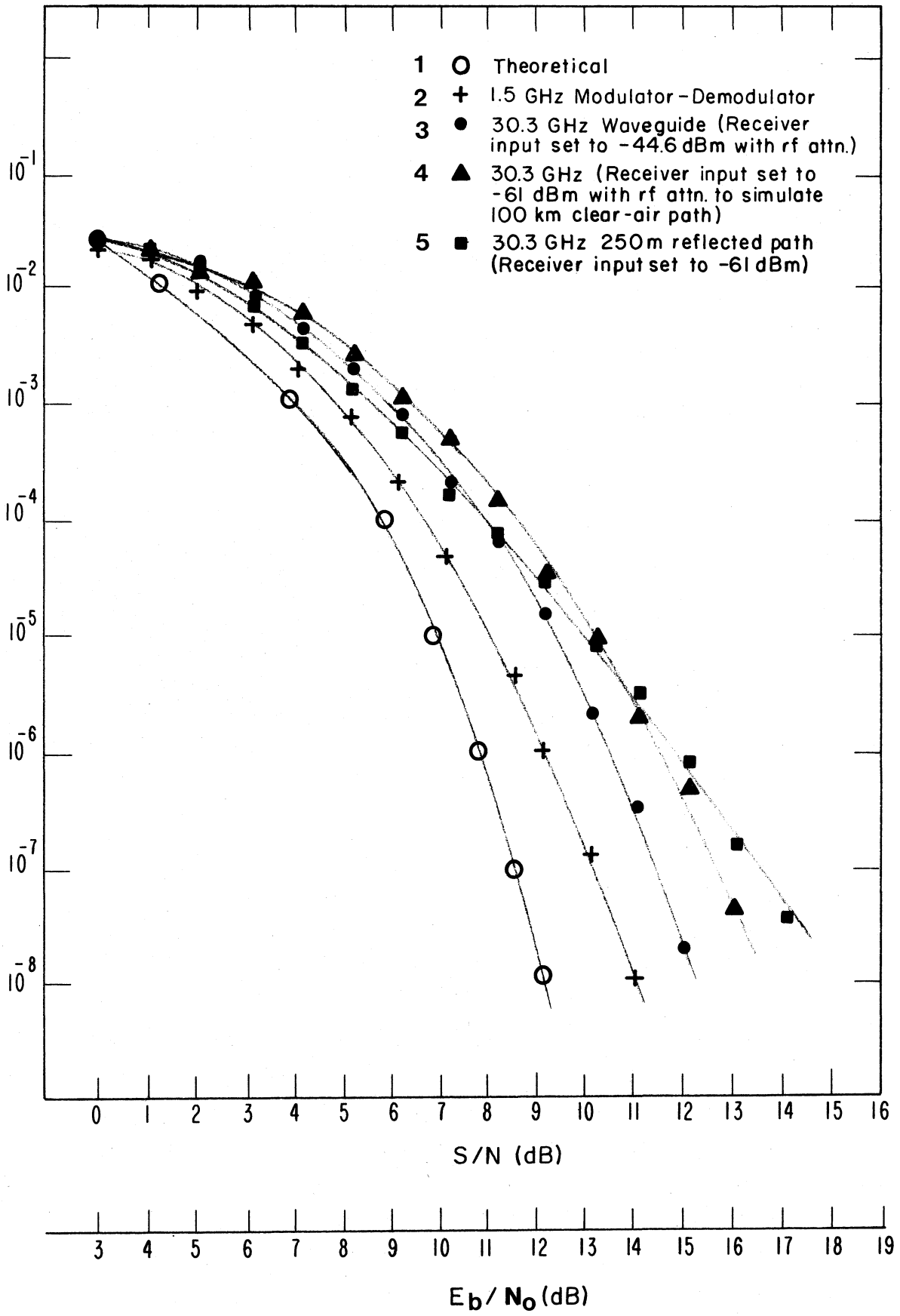

Figure 3.1 Plots of BER vs. E_b/N_o for several system configurations.

greatly in achieving this performance. Matched filters are adjusted for optimum BER at an E_b/N_o of 6 dB for the curves shown, consistent with the probe's use as a diagnostic tool. When the filters are optimized at an E_b/N_o of 13 dB, the maximum departure from the theoretical curve for modulator-demodulator is about 1.5 dB.

The third BER curve of Figure 3.1 indicates performance with the 30.3 GHz up-converter, the wide-band 30 GHz amplifier, and the receiver downconverter connected through about 15 feet (4.5 m) of WR-28 waveguide. A departure of about 3 dB from the theoretical curve occurred, with the greatest contributor to increased errors being the dispersion in amplitude and phase of the 26 to 38 GHz power amplifier. The input level to the receiver downconverter (balanced strip-guide mixer) was -75 dBm for the plot shown in curve #3.

The local oscillator signal for the downconverter is generated by a phase-locked, cavity-tuned multiplier and a low-noise resistive-type waveguide tripler stage; even so, the LO phase noise provides the noise figure limitation at the receiver. With the input level to the receiver reduced to -90 dBm, the LO phase noise just begins to cause an increase in the number of errors as shown in curve #4 using the waveguide link. The LO phase noise was not included as part of the E_b/N_o in plotting this curve.

Curve #5 results from a 250 meter folded path through the atmosphere using 3-foot (91 cm) dishes for both transmitting and receiving, with a 56 cm trihedral (90° corner) reflector. Again, the input to the receiver upconverter was set at -90 dBm which is equivalent to the received level for a 100 km clear-air path assuming atmospheric absorption to be 0.12 dB/km. As seen by the small separation in curves #4 and #5, neither the antennas, the 250 meters of atmosphere, nor the corner reflector produced appreciable degradation in received signal. Curve #5, over the short atmospheric path, becomes the reference for relative S/N and/or distortion over a path under test. Long term stability or the ability to reproduce the BER performance curve has been within the measurement accuracy of the power meter or about $\pm$ 1/4 dB.

4. BER PERFORMANCE IN THE PRESENCE OF CONTROLLED MULTIPATH

To produce a multipath signal, a second corner reflector (31 cm on a side) was mounted on an adjustable track to provide movements in line with the folded path by means of a 1 cm per revolution worm-drive mechanism. The adjustable track is centered at a point adjacent to the 56 cm reflector, which allows for a $\pm$ 120 cm position change or a $\pm$ 240 cm folded path length variation. At the reflectors, 125 meters away, the radii of the transmitting and receiving antenna beams are

approximately 0.9 meters at the 1/2 power points. The strength of the multipath signal is controlled by the relative position of the adjustable reflector in the antenna beam. A photograph of the two corner reflectors mounted on the roof of the Department of Commerce Radio Building is shown in Figure 4.1(a). Figure 4.1(b) shows a view from the reflectors looking toward the transmitting and receiving antennas. The sketch in Figure 4.1(c) shows the positioning of the transmitting and receiving antennas and the two reflectors.

Using the stationary reflector and movable reflector configuration to produce multipath, data was gathered for a continuous second reflector displacement of roughly $\pm$ 50 cm. When a folded path is used, the actual path length change is twice the physical separation in line with the path. Each 30 cm of path length change is very nearly 1 nanosecond in transit time difference. One such data plot is shown in Figure 4.2 where both received signal amplitude and BER are displayed relative to the transit time delay between reflected signals or as "multipath delay." A negative delay indicates that the multipath signal has a shorter round-trip time than the fixed reflector signal. The signal amplitude scale corresponds to the 20 dB AGC range of the demodulator; where in this test configuration, 10 dB is equivalent to a -69 dBm input to the receiver. Near the zero delay time, the signal amplitude has a cyclic variation in delay time equivalent to the period of the rf carrier or 0.033 ns, and a dB excursion that depends on the relative ratio of the received signals from the two reflectors. These excursions, of course, are the enhancements and fades that are typical of a path with multipath signals and results from constructive and destructive phase interference between received signals. For the data in Figure 4.2, the ratio of the reflected signals (R_1/R_2) is 7 dB.

At near zero delay, the BER curve also has a cyclic variation with a period equal to the rf period of 0.033 ns, but of a phase opposite to the signal amplitude variations. This BER pattern is produced almost entirely by the S/N variation, because little baseband signal distortion occurs when the multipath delay is small relative to a bit duration. The BER change in this delay range follows closely the BER versus S/N pattern shown in curve #3 of the E_b/N_o (S/N) versus BER plot of Figure 3.1. Curve #3 for the waveguide path provides a best fit for the single reflector folded path, instead of curve #5, because for this measurement the rf input level was sufficiently high that the front end noise did not produce bit errors. Bandpass noise was added to the received signal by the link performance tester to increase the BER to a convenient recording level. With only the fixed reflector in place the S/N was set at 11 dB which corresponds to an E_b/N_o of 14 dB

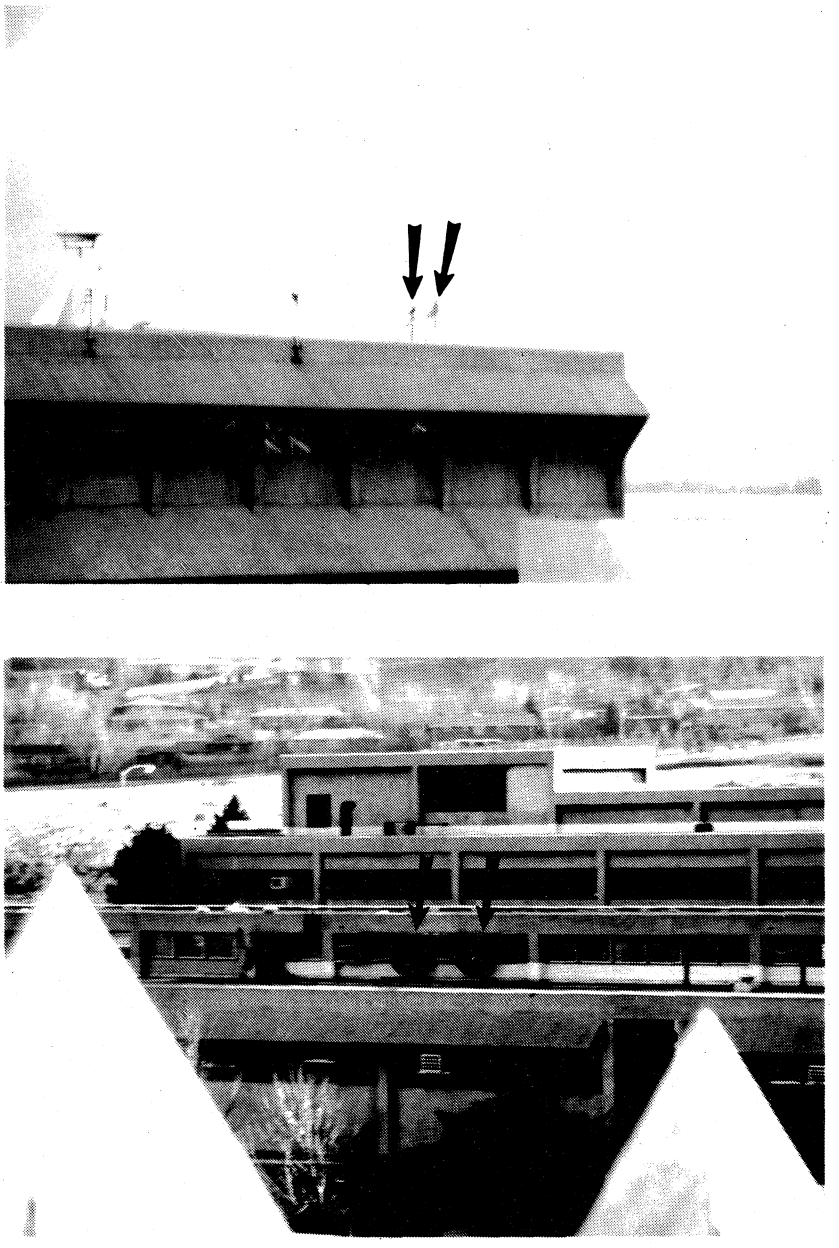

Figure 4.1 Photographs and a sketch of the experimental 250-meter folded path.

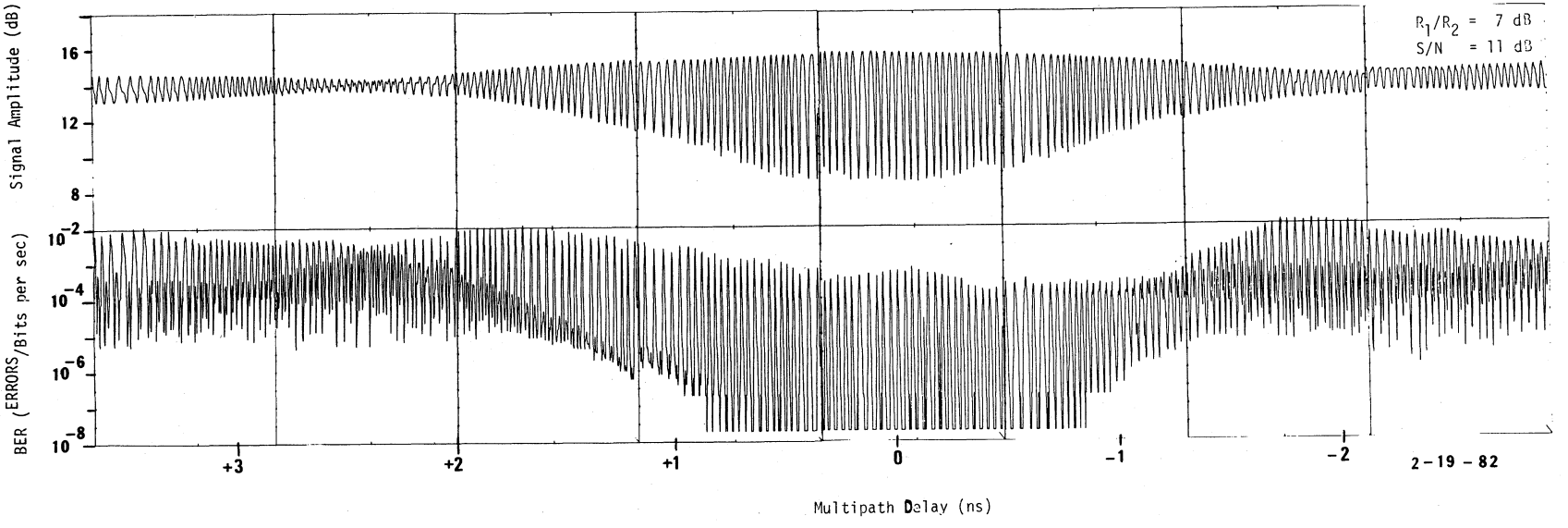

Figure 4.2 Received signal amplitude and bit error rate in the presence of a multipath signal (R_1/R_2 = 7.0 dB S/N = 11 dB).

and a BER of 8×10^{-7} as the no multipath reference level. For these tests the data acquisition system was capable of recording BER to 2×10^{-7} with the one second gate time used, and all BER less than this are arbitrarily set at 2×10^{-8}.

In Figure 4.2, the BER continues to increase from the zero delay point as a result of increasing intersymbol interference while the signal amplitude changes are decreasing, thus reducing the S/N variations. The signal amplitude variations diminish until the end of one bit duration (2 ns) because of the random binary code within the 2^7-1 bit word used for PSK modulation of the carrier. A residual signal variation of about 1 dB occurs due to the presence of a non-random component of the bit stream, a vestigial signal for carrier recovery, and a multiple of the bit clock frequency (500 MHz) mixing in the upconverter to give a 30.3 GHz sum. The phase of these small carriers are different which accounts in part, for the complex BER waveform seen beyond 2 ns in delay time.

Bit error rates resulting from intersymbol interference are also dependent on the S/N of a digital system since the delayed component will change the primary signal phase for a portion of each bit time causing the phase detected output voltage envelope at baseband to vary for all or part of it's duration. A reduced S/N increases the probability of a noise vector combining to cross the decision boundary producing an error. A plot of BER versus multipath delay is shown in Figure 4.3 for a R_1/R_2 of 8 dB and S/N values of 22.4, 17.4, and 12.4 dB.

A multipath delay which approximately coincides with one bit time (2 ns) is examined. If in Figure 3.1, curve #3 is referenced at an S/N of 22.4 dB, the BER would be less than the 1×10^{-8} if the signal amplitude changes in Figure 4.3 alone were responsible for the errors. All BER peaks correlate with minimum signal amplitude levels and BER minimums correlate in time with the peaks of the signal amplitude. Note that a secondary cyclic variation at the rf rate appears in the lower two S/N plots of the BER. As will be seen in subsequent data, these become the dominant BER changes as the multipath delay increases.

The periods of the amplitude and BER peaks are not uniformly spaced in these figures because the data were recorded while the movable reflector was cranked slowly by hand and it was not possible to maintain a constant rate. Each of the three plots of Figure 4.3 were separate scans, yet the signal amplitude repeatablity is good considering the distance traveled between peaks is 0.5 cm ($\lambda/2$). Figure 4.4 shows the BER for the same three values of S/N as in Figure 4.3 except that the multipath delay is near 3 bit durations (6 ns). Here the amplitude variations are only slightly greater than 1 dB, but it is clear that the dominant BER peaks and minimums do not correlate with the amplitude excursions. In this case the secondary

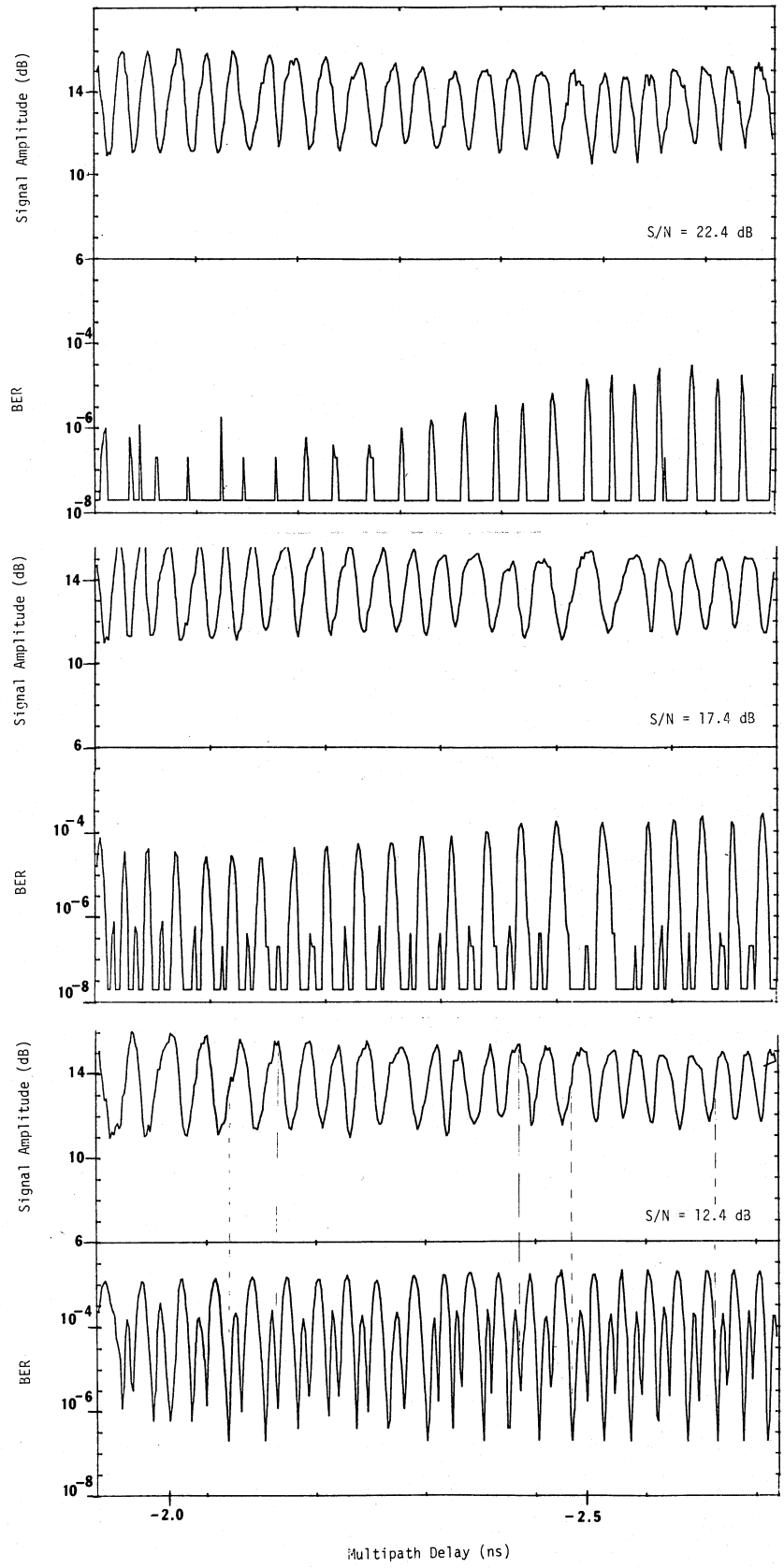

Figure 4.3 Received signal amplitude and bit error rate multipath delay at about one bit duration with S/N of 22.4 dB, 17.4 dB, and 12.4 dB.

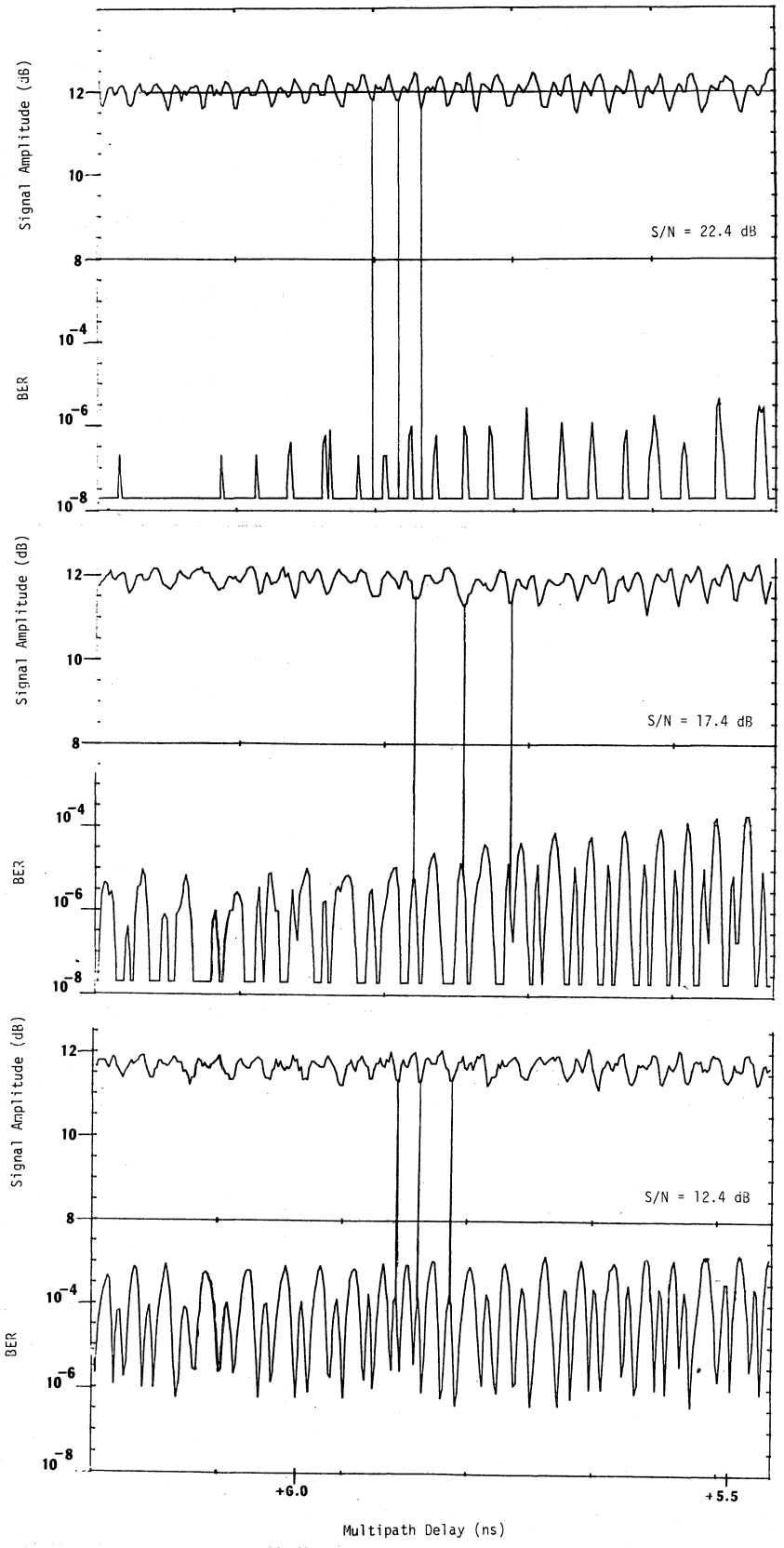

Figure 4.4 Received signal amplitude and bit error rate for multipath delay at greater than one bit duration with S/N of 22.4 dB, 17.4 dB, and 12.4 dB.

BER peaks now correlate with the amplitude minimums. Even though the average signal level does not change appreciably with multipath delay due to the random binary word, each bit period has a constructive and destructive interference cycle which depends on the relative rf phase between the direct and multipath signals. Since all signals (baseband through rf) are coherent, the occurrence of the rf fades and enhancements produce baseband detected output changes at the rf rate.

The decision time is the time at which the baseband phase detector output is sampled to determine whether a "one" or "zero" is present. This decision time is adjusted for minimum BER during normal channel conditions which generally occur at a point sometime after a half bit duration to allow leading edge transients to settle. With multipath interference present the baseband phase detector output voltage (at the decision time) varies at the rf interference rate, contributing to the cyclic pattern of the BER when the delay times are beyond one bit duration. The automatic gain control circuitry cannot respond during the 1 to 2 ns bit duration but requires many bit durations to adjust the amplifier gain (Figure 2.3). In addition, the phase of the reconstructed carrier which is adjusted by the phase shifter (Figure 2.3) is also changed by the presence of a multipath signal. The phase change of the reconstructed carrier reference signal is the other contribution to the cyclic variation of BER as the multipath delay is continuously varied.

To obtain a measure of the effect of a smaller multipath level, a plot of signal amplitude and BER versus multipath delay with a R_1/R_2 of 13 dB and an S/N of 12 dB is shown in Figure 4.5. At a delay greater than one bit time, the average BER tends toward 2×10^{-5}, whereas a BER of 3×10^{-8} occurred with only the fixed reflector in path.

5. IMPULSE RESPONSE AND AMPLITUDE DISPERSION MEASUREMENTS IN THE PRESENCE OF CONTROLLED MULTIPATH

In order to isolate fade and distortion mechanisms on a channel, the impulse probe is most useful. Impulse response measurements can be applied to a channel to predict BER and to assist in operational system design questions, such as, can space diversity or adaptive equalization be utilized to improve performance. Also, if an ensemble of impulse response data is recorded, the dynamics of the channel transfer function can be determined for performance prediction.

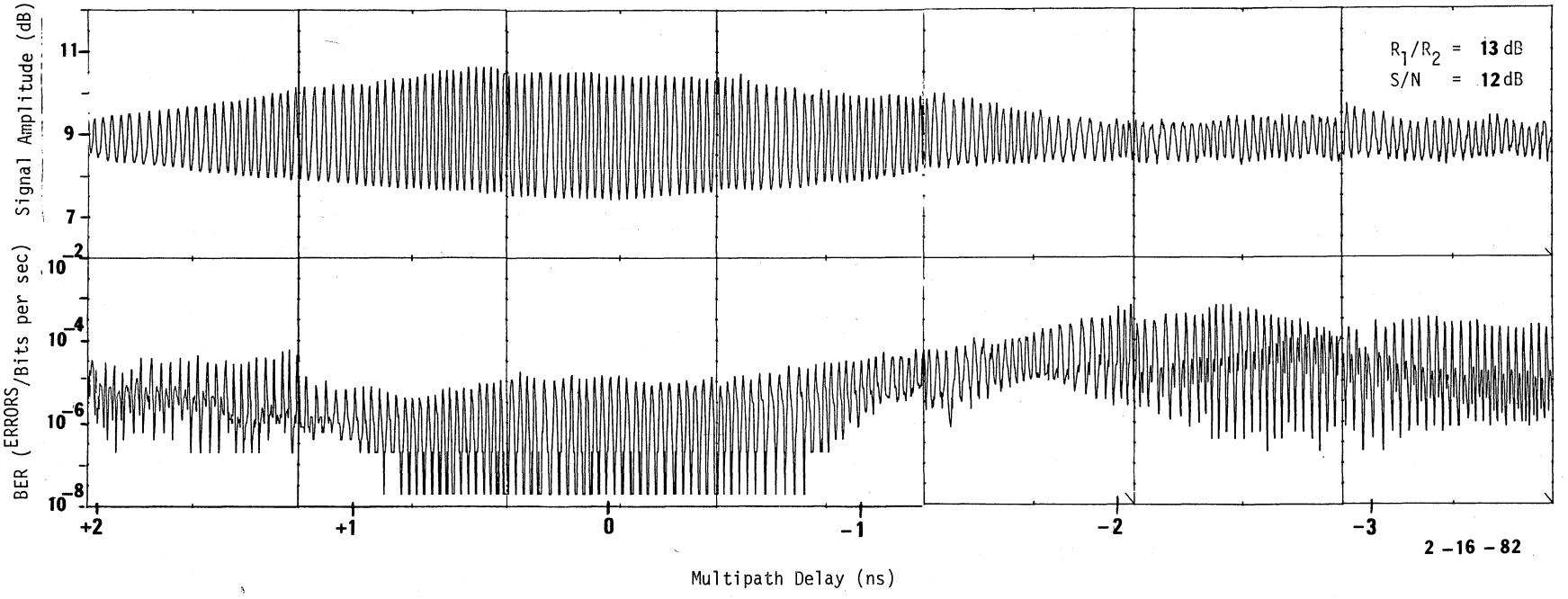

Figure 4.5 Received signal amplitude and bit error rate for multipath (R_1/R_2 = 13 dB, S/N = 12 dB).

In the controlled multipath experiment, the impulse probe was used to observe the conditions that produce the BER data described above. Figure 5.1 is the impulse response of the channel for the condition of Figure 4.4 at a point where the multipath delay is 6 ns. A one nanosecond delay is approximately equivalent to 1 foot (30.5 cm) of additional path length. In the experiment, the vertices of the corner reflectors were separated 3 feet (0.91 m) (equivalent to 6 feet two-way distance) for the impulse recording. The R_1/R_2 ratio was 8 dB. After balancing the mixer-correlators and the sum of the squares circuitry, the multipath signal amplitude agrees with measured R_1/R_2 to within $\pm$ 1.5 dB as the delay is varied through an rf cycle. The largest source of error is the nonlinearity of the correlators with amplitude change, but these are state-of-the-art at this time. Design techniques to improve linearity and frequency response of these correlator-mixers are being continued by manufacturers and these items can be expected to provide better performance as improved units become available. For the multipath condition of R_1/R_2 = 8 dB, 6 ns delay, and an S/N ratio of 12.4 dB as shown in Figure 5.1, a BER of 5×10^{-5} was observed. This value compares to 2×10^{-8} for the same path with the same S/N ratio and no multipath (single reflector).

An amplitude response from a spectrum analyzer of a signal with a 2 GHz subcarrier bandpass gives an indication of the signal level dispersion occurring on a millimeter wave channel. A frequency spectrum containing a line every 4 MHz (2^7 bits per word) is shown in Figure 5.2(a) for a single reflector folded path to show the amplitude response when no channel distortion is present. The spectrum analyzer is centered at 1.5 GHz distinguishable by the cw carrier spike. In Figure 5.2(b) for the same path, the second reflector is in place to give a 6 ns delayed signal. The spacing between fades is about 160 MHz (0.1667×10^{-9}) and the null depth at either side of 1.5 GHz can be read as approximately 7 dB, which substantiates the controlled parameters (4.4 dB fade and 2.9 dB enhancements).

A second set of signal spectra is shown in Figure 5.3, with corresponding impulse response curves. A spacing between reflectors of about 4 inches (10 cm) was set, again using the same R_1/R_2 of 8 dB. The data in Figure 5.3 show the impulse response of the single reflector case as a solid line and spectrum response (a). With injected noise, the BER was set at 1.6×10^{-7} for the single reflector. With the addition of the second reflector, which produced a multipath signal of about 0.6 ns delay, the BER was increased to 5×10^{-6}. The dashed line portion of the impulse response shows the 0.6 ns delay with a 0.5 dB amplitude enhancement. Where the impulse of the multipath overlaps the impulse of the direct path at its

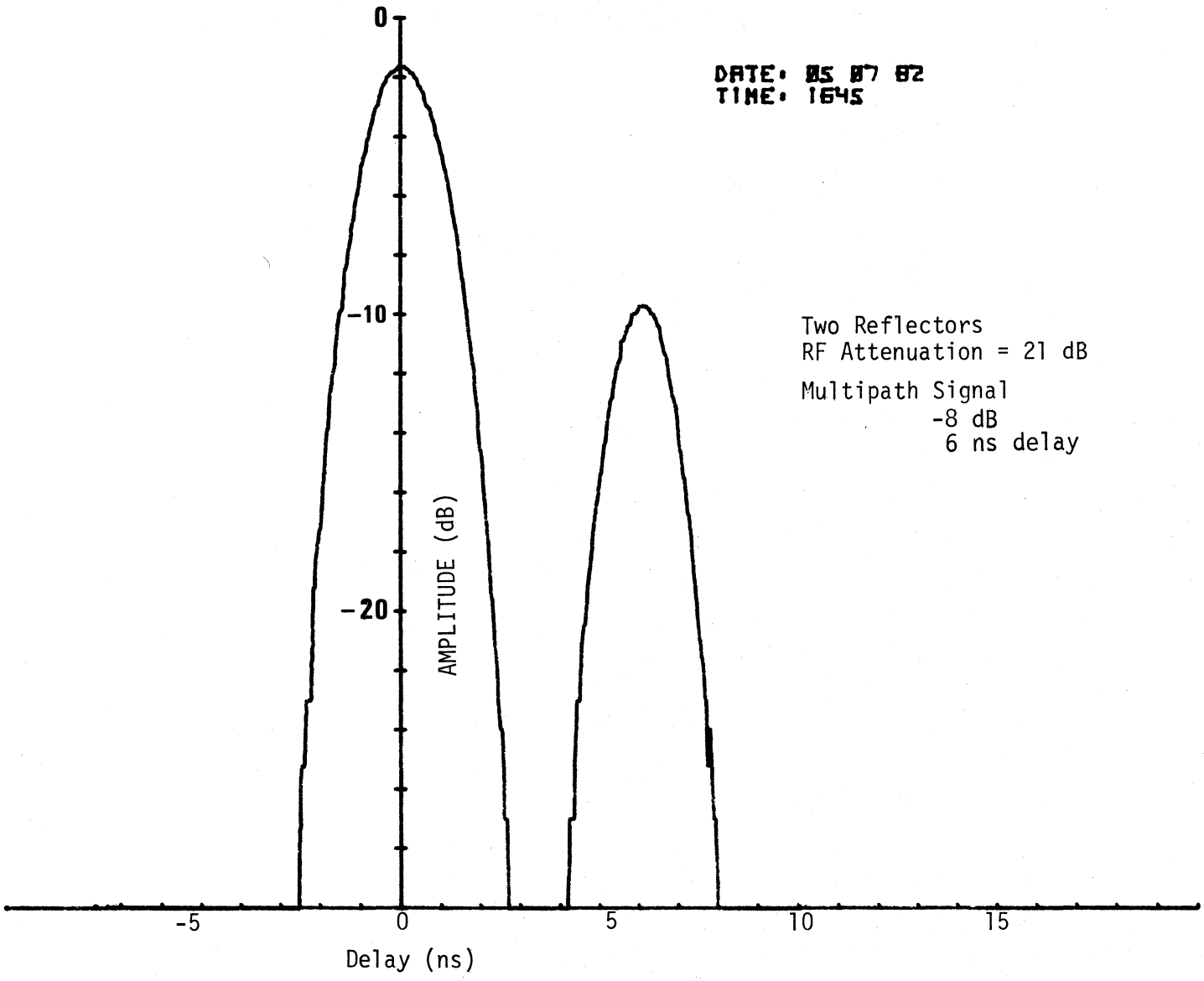

Figure 5.1 An impulse response with two reflectors, the multipath occurs at 6.0 ns with relative amplitude of -8.0 dB.

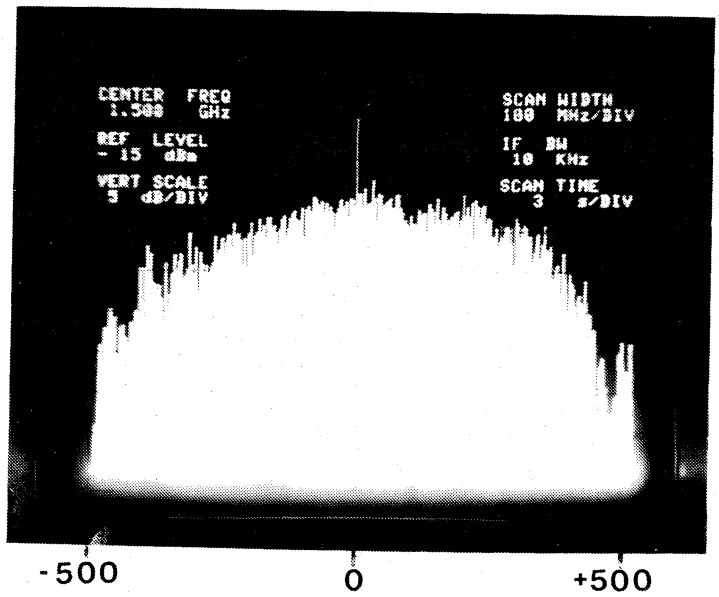

a) Single Reflector 250 m (folded) path
RF Attenuation = 40 dB
BER = 1×10^{-6}

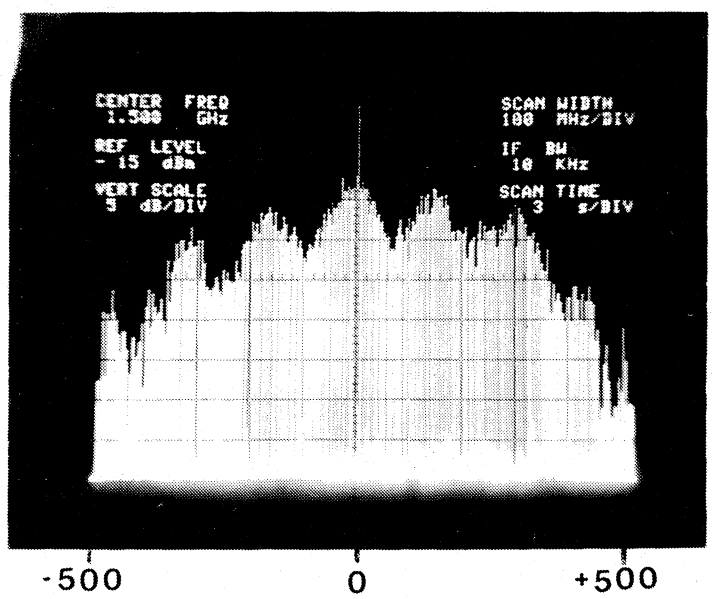

b) Two Reflectors 250 m (folded) path
RF Attenuation = 40 dB
BER = 2×10^{-4}
Multipath Signal -8 dB, 6 ns delay

Figure 5.2 Frequency spectra of received signal with a single reflector and with two reflectors.

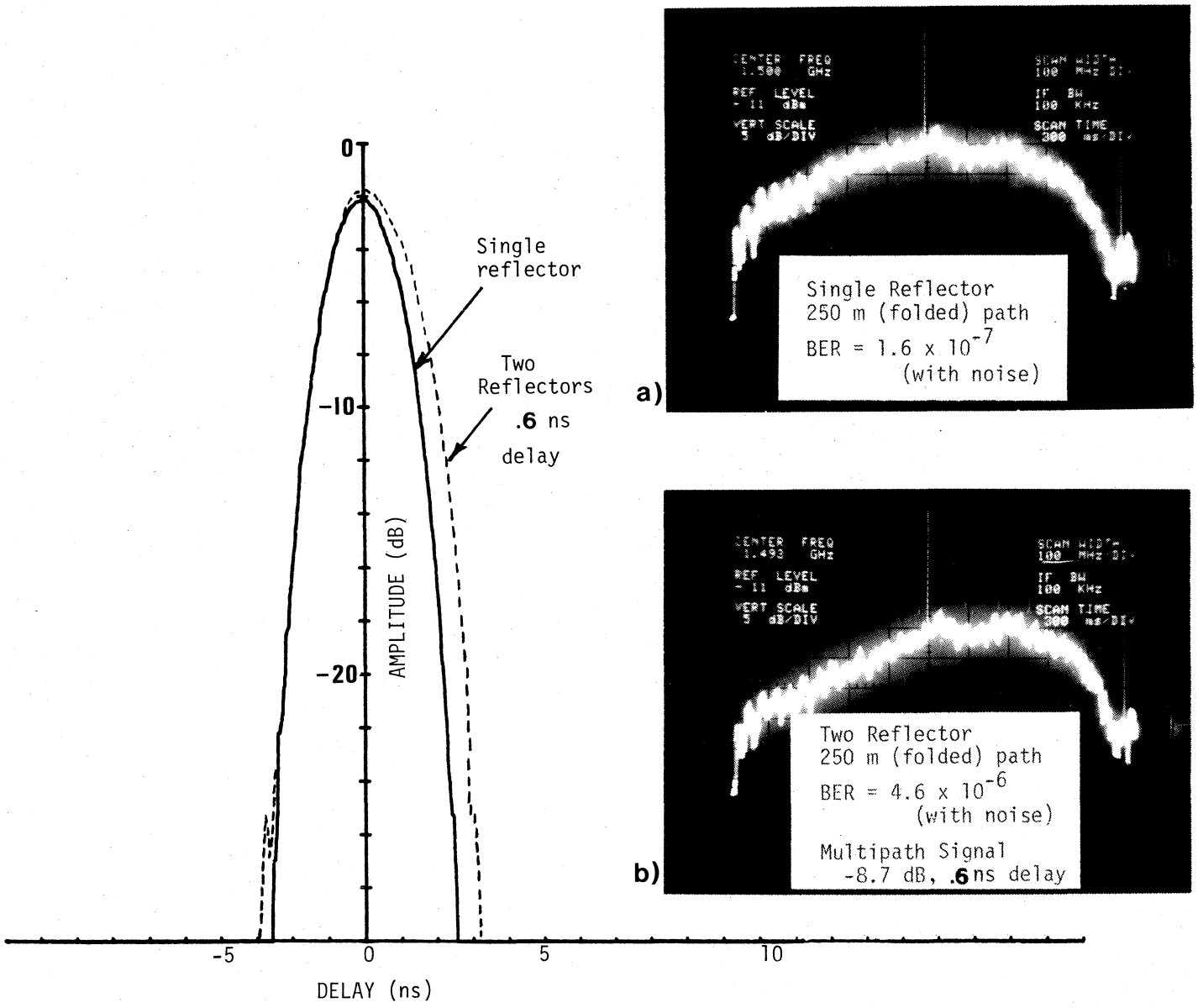

Figure 5.3 Impulse response curves with corresponding spectra with a single reflector and with two reflectors on a 250-meter folded path.

center, it is necessary to use processing techniques to derive the multipath amplitude (El-Behery and MacPhie, 1980). The software is yet to be completed at this writing to show accuracy of this procedure. For the overlapping case the extension of the base at the -30 dB axis approximates the delay time.

The spectrum response in the lower photograph (b) shows the fade falling outside the bandpass, and only a distorting tilt is seen in the signal spectrum. The fade nulls in this case are spaced each 1.66 GHz for a 0.6 ns delay. A 2^{15} bit word length was used for these frequency scans which provides a line approximately each 15 kHz resulting in considerably better resolution.

6. EFFECTS OF MULTIPATH ON DIGITAL LINK PERFORMANCE

Multipath data taken on the 250 meter folded path, using the 30.3 GHz, 500 Mb/s coherent BPSK is compiled to give a view of multipath effects. Figure 6.1 contains a plot of contributions to BER by S/N variations and intersymbol interference as a function of the time delay of a multipath signal relative to the direct signal normalized to bit duration. For this plot, the direct-to-multipath signal ratio (R_1/R_2) is 7 dB. With no multipath present and a 11 dB signal-to-noise ratio, the BER is 5×10^{-7}. At zero multipath delay the change in BER is due only to S/N changes with an average BER of about 1.5×10^{-6}. This average BER is greater than the no multipath case because fades of 5.1 dB and enhancements of only 3.2 dB occur for a R_1/R_2 of 7 dB. Since a psuedo-random sequence bit generator is used to produce the data stream, the amplitude variations diminish as the multipath delay extends to one bit duration (see Figure 4.2). Hence, the errors due to S/N change as shown by the narrow hatched lines marked, "BER due to S/N only." Amplitude variations as a result of multipath at delay times greater than one bit duration are small. Some additional amplitude variation in the system is due to cw components in the signal used for reconstructing the carrier.

Errors due to intersymbol interference for this multipath case (Figure 6.1) are shown to diverge from zero delay, beginning at the BER (5×10^{-7}) for a no multipath state. This indicates that there is no intersymbol interference contribution at zero multipath delay relative to the direct signal. As the multipath delay increases, the maximum and minimum contribution from intersymbol interference is shown by the broad-spaced hatch lines extending to coincide with the total contribution of errors at a delay time equal to one bit duration. Part of the errors attributed to intersymbol interference are the result of the composite of the direct signal and multipath signal producing a phase shift in the reconstructed carrier. As shown in Figure 2.3, the reconstructed carrier is manually phase

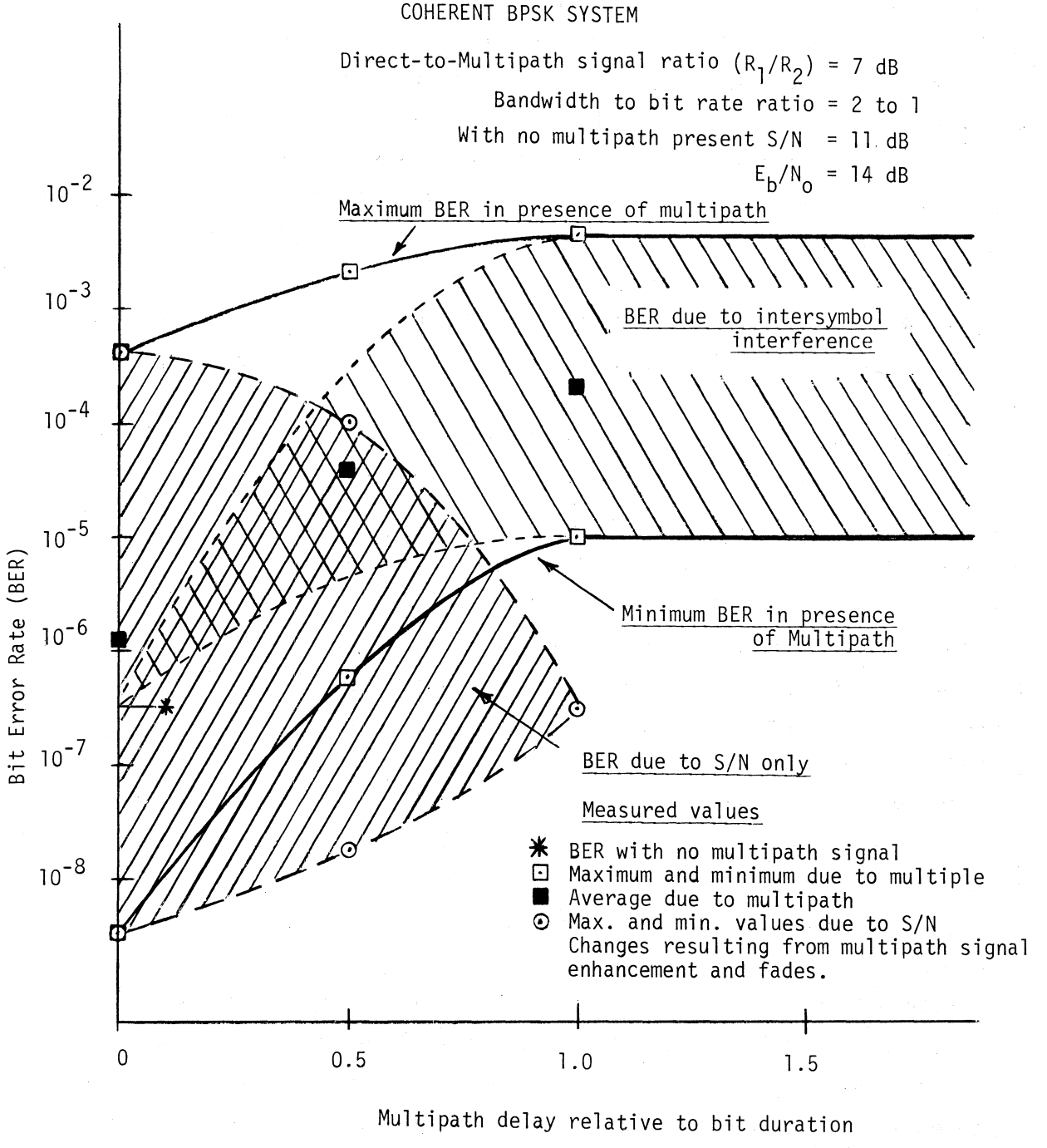

Figure 6.1 BER in the presence of multipath signals due to S/N and to intersymbol interference for a S/N of 11 dB and a direct-to-multipath signal ratio of 7 dB.

adjusted to provide a zero reference to the phase detector in the demodulator for recovery of the baseband signal. This composite signal phase shift is cyclic at the rf rate and the resulting phase error accounts for part of the maximum-minimum BER excursions. A similar process occurs with the reconstruction of the bit rate clock (Figure 2.4), which is also modulated at the rf rate by multipath signals, but is the result of intersymbol interference.

A second technique to reconstruct the carrier by multiplying the PSK or QPSK modulated carrier by four to produce an unmodulated reference was tested. A voltage controlled oscillator at the carrier frequency was phase-locked to the times 4 output to provide the reference carrier. This means of generating the reference carrier produced the same maximum and minimum BER excursions as the injected carrier technique, but for QPSK modulation four possible phase-lock states exist, with only one correct. Excessive time was required to obtain carrier lock-up and data word synchronization, which was unsuitable for the intended flexible operation of the probe.

The BER due to a multipath signal is dependent on the channel S/N and the strength of the multipath signal. For a direct-to-multipath signal ratio of 8 dB, Figure 6.2 shows measured and extrapolated values of BER as a function of S/N compared to a curve showing system performance without a multipath signal. All values plotted are for a case where the multipath signal delay is one bit duration or greater. The measured points using the passive reflectors to generate multipath are indicated by the small circles on the figure. These points include minimum, average, and maximum BER as a result of the multipath signal being continuously varied in delay time over several rf cycles.

Bit error rate versus S/N curves are extrapolated from measured data, for three different ratios of direct-to-multipath signal level in Figure 6.3. An estimated scale of R_1/R_2 starting at 7 dB and extending to ∞, which is the no multipath state, is included for the case where the multipath delay time is one bit duration or greater.

Multipath signals in a high data rate channel have a serious effect on data transfer rates due to increased errors. This treatment of multipath involving a single discrete signal may not always be representative of an actual path. Several components of multipath may occur or numerous scatters may exist such as reflections from irregular terrain. However, the measurements made for this report will provide a good reference of channel degradation for the conditions which may be encountered on atmospheric paths, say, 5 km or more in length. More important is

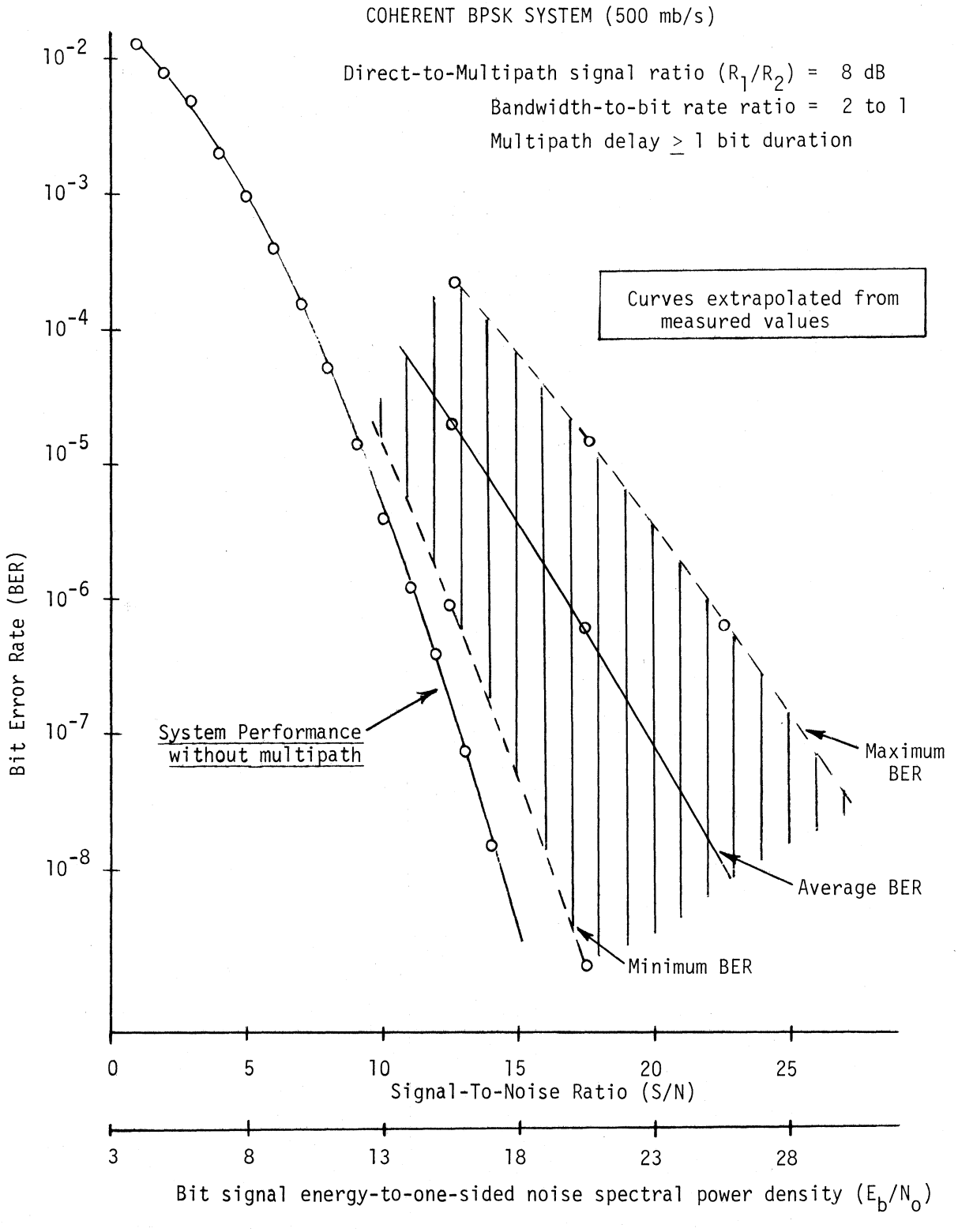

Figure 6.2 BER as a function of S/N for a direct-to-multipath signal ratio of 8 dB for multipath delays greater than 1 bit duration.

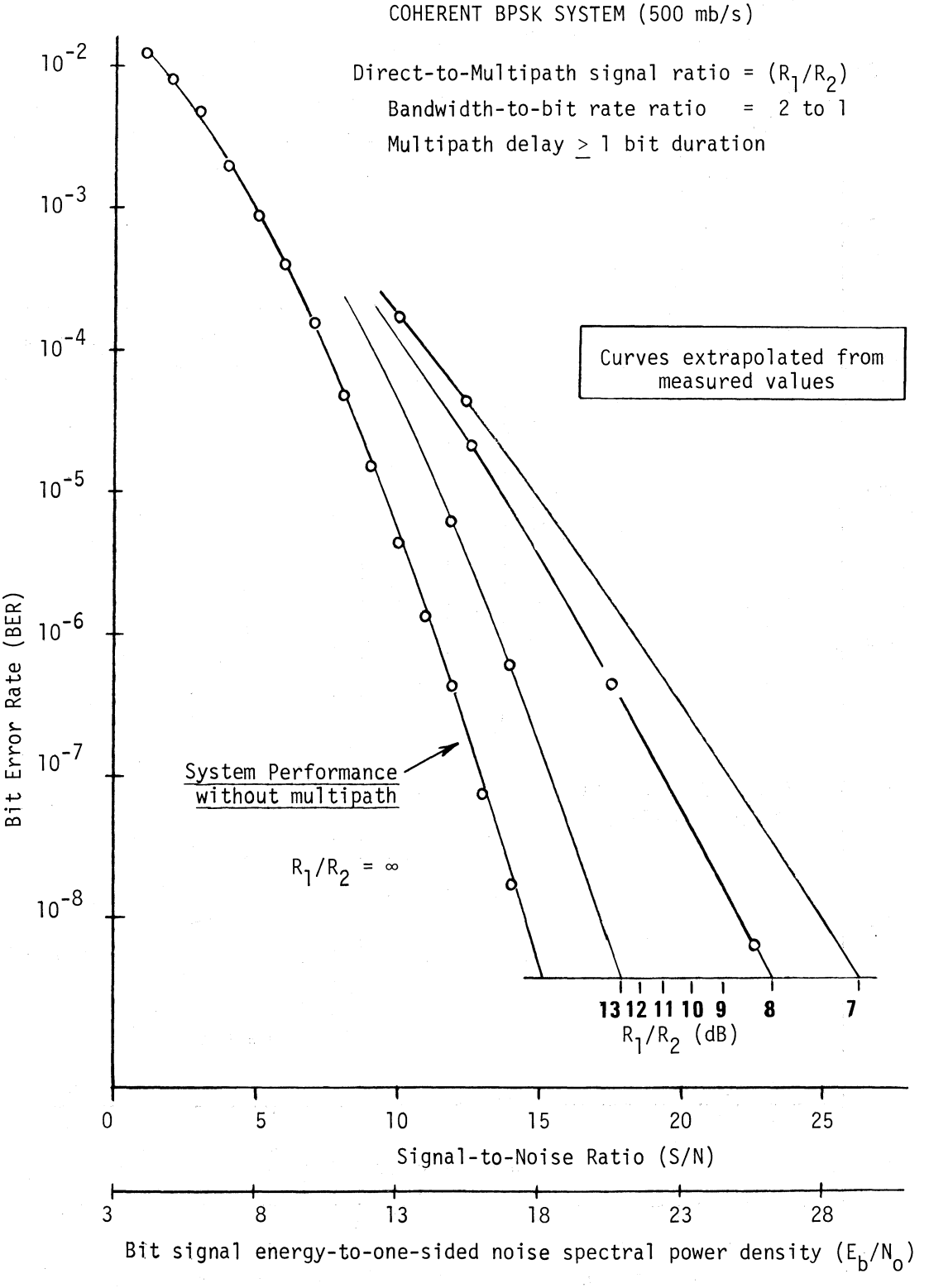

Figure 6.3 BER as a function of S/N for direct-to-multipath signal ratios (R_1/R_2) from 7 to 13 dB for multipath delays greater than 1 bit duration.

the insight obtained from these measurements when the diagnostic probe is applied to long paths for purposes of performance analysis.

7. SUMMARY

Since the diagnostic probe is portable (in that the terminals fit in small vans with adjustable antenna carriages) and has data acquisition and timing under computer control, it can measure performance parameters of a variety of contemplated paths. Some paths to be examined will have trees illuminated by the antennas or actually obstructing the path. In urban environments buildings will be in or near the path. For these conditions the impulse probe will provide a direct view of the time delay spread of the signal to obtain data on absorptive, reflective, and diffractive characteristics as well as resulting BERs. For LOS atmospheric paths, the wideband portion of the diagnostic probe can provide BER information, record periods of anomalous propagation, and identify the propagation anomalies by either the impulse response or amplitude dispersion measurements. Since the diagnostic probe includes coherent rf channels below and above the wideband channel, frequency dependence of fades or distortion mechanisms can be observed to aid in their identification. These mechanisms, include multipath, defocusing, beam decoupling, a result of atmospheric refractive ray bending on a LOS path, and absorption and diffraction from hydrometeors in the air.

Millimeter wave channels are rapidly becoming very economical in terms of dollars/Hz bandwidth, particularly if the channel quality is adequate without using adaptive equalizers or space diversity techniques. These techniques become difficult to design and expensive for wide-band systems and should be avoided if performance requirements can otherwise be met. The diagnostic probe applied to a channel can provide design criteria and performance data; within the constraint of observation time for statistical evaluation, to determine the improvement expected from such techniques within the 30 to 100 GHz frequency band.

Once a sufficient number of measurements are made for different climatic regions and environmental situations, existing models can be verified or new models generated to predict performance of a given link. One such set of measurements using the wideband diagnostic probe during July 1982 on an 11.8 km path is discussed in a report entitled "Millimeter Wave Wideband Diagnostic Probe Measurements at 30.3 GHz on an 11.8 km Link" (Espeland, et al., unpublished as of this date). These measurements show the interaction of multipath signal and bit error rates resulting from an induced ground multipath.

8. REFERENCES

El-Behery, I.N., and R.H. MacPhie (1980), The resolution limit of a variable baseline synthetic aperture antenna, IEEE Trans. Ant. Prop. AP-28, pp 234-238.

Furuhama, Y., and T. Ihara (1981), Remote sensing of path-averaged raindrop size distributions from microwave scattering measurements, IEEE Trans. Ant. Prop. AP-29, pp 275-281.

Gray, J.S. (1969), Signal conditioning, bit synchronization, and group synchronization for high bit rate PCM, National Telemetry Conference, Washington, D.C.

Gray, J.W. (1972), Signal processing for digital communications for a 1 Gb/s data rate, International Communications Conference, Philadelphia, PA.

Gray, J.S. (1973), Laser Transceiver Electronic I, Technical Report AFAL-TR-73-282, Air Force Systems Command, Wright-Patterson Air Force Base, OH.

Hufford, G.A., R.W. Hubbard, L.E. Pratt, J.E. Adams, and S.J. Paulson, NTIA and P.F. Sass (1982), Center for communication systems, wideband propagation measurements in the presence of forests, CECOM 82-CSO29-F, Appendix A, January.

Linfield, R.F., R.W. Hubbard, and L.E. Pratt (1976), Transmission channel characterization by impulse response measurements, OT-Report 76-96, August.

Wozencraft, J.M., and I.M. Jacobs (1965), Principles of Communications Engineering, (John Wiley and Sons, Inc., New York, NY), p 83.

FORM **NTIA-29**
(4-80)

U.S. DEPARTMENT OF COMMERCE
NAT'L. TELECOMMUNICATIONS AND INFORMATION ADMINISTRATION

BIBLIOGRAPHIC DATA SHEET

	1. PUBLICATION NO.	2. Gov't Accession No.	3. Recipient's Accession No.
	NTIA Report 83-128		

4. TITLE AND SUBTITLE
A Diagnostic Probe to Investigate Propagation at Millimeter Wavelengths

5. Publication Date
August 1983

6. Performing Organization Code

7. AUTHOR(S)
E.J. Violette, R.H. Espeland, K.C. Allen

9. Project/Task/Work Unit No.

8. PERFORMING ORGANIZATION NAME AND ADDRESS
U. S. Department of Commerce
National Telecommunications & Information Administration
Institute for Telecommunication Sciences
Boulder, Colorado 80303

10. Contract/Grant No.

11. Sponsoring Organization Name and Address
same

12. Type of Report and Period Covered

13.

14. SUPPLEMENTARY NOTES

15. ABSTRACT *(A 200-word or less factual summary of most significant information. If document includes a significant bibliography or literature survey, mention it here.)*

A diagnostic probe used to fully describe the propagation characteristics of a millimeter wave channel by nearly simultaneous recording of an impulse response, frequency spectra, amplitude response, and bit error rate is discussed. A 30.3 GHz carrier accommodates the subcarriers and baseband modulation modes in a fully coherent network. Signal-to-noise determining components will permit BER performance of better than 10^{-8} at a 500 Mb/s rate with a 25 dB fade margin through a clear air 50 km distortion free path. Back to back operation of the terminals and a short atmospheric path is used to establish the reference performance level of the hardware. Controlled multipath tests are reported to demonstrate probe capabilities and to obtain reference data to better classify the fades and resulting distortion which occur on terrestrial links at millimeter wavelengths. With dual reflectors, multipath data sets were compiled to aid in predicting bit error rate performance resulting from a combination of signal-to-
continued

16. Key Words *(Alphabetical order, separated by semicolons)*
Diagnostic; digital; millimeter waves; propagation; probe; wide-band

17. AVAILABILITY STATEMENT
☒ UNLIMITED.
☐ FOR OFFICIAL DISTRIBUTION.

18. Security Class. *(This report)*
unclassified

20. Number of pages
38

19. Security Class. *(This page)*
unclassified

21. Price:

☆ U.S. Government Printing Office: 1980—678-495/529

noise ratio change and intersymbol interference. Included with the above data are corresponding measurements of the impulse response and amplitude distortion on the channel. Two additional coherent cw channels, 11.4, 28.8, and a soon to be added 96.1 GHz channel, are included with the 30.3 GHz probe to aid in analyzing selective fades that fall outside the bandpass and to evaluate frequency dependent properties of a link.

☆ U.S. GOVERNMENT PRINTING OFFICE: 1983—680-909/443 REGION NO. 8